Interannual and Intra-seasonal Oscillations in the Length of Day, Atmospheric Angular Momentum and Atmospheric Surface Pressure Time Series Observed at Chosen Meteorological Stations Near the Equator

Lihua Ma
National Astronomical Observatories Chinese Academy of Sciences
Wieslaw Kosek (wieslaw.kosek@wat.edu.pl)
Wojskowa Akademia Techniczna im. Jaroslawa Dabrowskiego Wydzial Inzynierii Ladowej i Geodezji
https://orcid.org/0000-0002-1798-7097
Yanben Han
National Astronomical Observatories Chinese Academy of Sciences

Full paper

Keywords: length of day, atmospheric surface pressure, El Niño, wavelet transform, Fourier transform, Hilbert transform

Posted Date: July 9th, 2020

DOI: https://doi.org/10.21203/rs.3.rs-39392/v1

Interannual and intra-seasonal oscillations in the length of day, atmospheric angular momentum and atmospheric surface pressure time series observed at chosen meteorological stations near the equator

Lihua Ma[1], Wiesław Kosek[2*], Yanben Han[1]

1 National Astronomical Observatories, Chinese Academy of Sciences, Beijing, P.R. China

2 Faculty of Civil Engineering and Geodesy, Military University of Technology, Warsaw, Poland
[*] *Corresponding author: Wieslaw Kosek ORCID: https://orcid.org/0000-0002-1798-7097*

ABSTRACT The atmospheric surface pressure time series of Madras, Darwin, and Tahiti together with non-tidal length-of-day (LODR) variations and axial component of atmospheric angular momentum (AAM) were analyzed by wavelet transform as well as the combination of the Fourier transform band pass filter with the Hilbert transform (FTBPF+HT) to detect interannual and intra-seasonal oscillations in them. It was found that annual oscillations in the atmospheric surface pressure variations of Darwin and Tahiti stations are in phase and are about 180º out of phase in the atmospheric surface pressure variations of Madras station. The phase of the annual oscillation in atmospheric surface pressure variations of Madras station is slightly greater (~20º) than the phase of the annual oscillation in the LODR time series. The amplitude and phase variations of the annual and semi-annual oscillations computed by the FTBPF+HT combination in LODR and the axial component of AAM are very similar. The mean amplitudes of the semi-annual oscillation in the atmospheric surface pressure variations of Madras and Tahiti are of the order of 0.4 hPa, the phases of these oscillations are stable and the amplitude of the semi-annual oscillation in the atmospheric surface pressure variations of Darwin is negligible due to unstable phase of this oscillation. The atmospheric surface pressure variations of Madras, Darwin, and Tahiti stations show similar amplitude wideband signals with a central period of ~4 years (cutoff periods ranging from about 2.2 to 20 years) related to El Niño phenomenon. The amplitude maxima of this signal corresponding to the strongest El Niño events in 1982-83, 1997-98, and 2014-15 are also present in amplitude variations of this signal in the LODR and AAM χ_3 time series.

Keywords length of day, atmospheric surface pressure, El Niño, wavelet transform, Fourier transform, Hilbert transform.

1 Introduction

The Earth's variable rotation including variations of the length of day (LOD), polar motion, precession, and nutation is mostly caused by mass redistributions in different parts of the Earth system and the gravitational

torque exerted by the Moon and the Sun. Variations in the Earth's rotation described by polar motion and LODR variations, which are the LOD variations with zonal tide model removed, with respect to an Earth-fixed reference frame are mostly driven by redistribution and motion of masses within and between the atmosphere, the oceans, and land hydrology. The redistribution of mass generates changes in the Earth's inertia tensor, while the mass movement within the fluid layers relative to the solid Earth induces the exchange of angular momentum between these layers and solid Earth. Variations of LODR occur over a wide range of time scales from hours to a few years (e.g. Barnes et al., 1983; Ma et al., 2006a,b) and atmospheric winds and surface pressure changes explain about 90% of the LODR fluctuations (e.g. Gross et al., 2004). Oscillations with periods from about two to a few years in the LODR are excited by large-scale 2-7-year El Niño/Southern Oscillation (ENSO) of the global atmosphere-ocean system (e.g. Chao, 1984; Rosen et al., 1984; Salstein & Rosen, 1986; Dickey et al., 1992; Gambis, 1992). Gipson and Ma (1999) showed that during El Niño event 1982-83 an increase of LODR and the axial component of the atmospheric angular momentum (AAM) was noticed. Dickey et al. (1994) reported the presence of Quasi-Biennial Oscillation (QBO) of the equatorial stratosphere and 4-6 year oscillations related to ENSO in LODR and Chao (1989) showed better agreement QBO+ENSO combination with LODR time series. The annual and semi-annual oscillations excited by the axial component χ_3 of the AAM are the most remarkable components in the LODR changes (e.g. Frostman et al., 1967; Höpfner, 1998).

Long-term observational records of atmospheric surface pressure at some chosen meteorological stations including Madras, Darwin, and Tahiti near the equator, can provide some important information about the relationship between LODR data and surface pressure variations. To investigate relations between the atmosphere surface pressure data at these stations and the LODR time series, the wavelet technique, the Fourier transform band pass filter (FTBPF), and its combination with the Hilbert transform

(FTBPF+HT) were applied. The FTBPF+HT algorithms were also applied to investigate relations between LODR and surface pressure variations at Madras, Darwin and Tahiti stations and axial component χ_3 of the AAM time series.

2 Data

The daily LODR data since 1962.0 till now called eopc04R_IAU2000_daily available at the IERS (International Earth Rotation and Reference Systems Service) website (http://hpiers.obspm.fr/eoppc/series/opa/) was used in the analysis. To extend the LODR time series in the past from 1956.0 to 1962.0 the UT1-TAI data from EOPC01_IAU2000_(1900-now) with a 0.05-year sampling interval were used from which zonal tided model (IERS Conventions 2010) was removed and then UT1R-TAI data were converted to LODR time series.

The monthly atmospheric surface pressure observations monitored from January 1796 to March 2003 at the Madras station (Allan et al., 2002), and monthly atmospheric surface pressure observations at Darwin (since January 1866 till October 2019) and Tahiti meteorological stations and monthly normalized pressure difference (Southern Oscillation Index, SOI) between Tahiti and Darwin since June 1856 till October 2019 (Ropelewski & Jones, 1987) were used in the analysis (http://www.cru.uea.ac.uk/data). The atmospheric surface pressure data at Madras, Darwin, and Tahiti stations are called in this paper as APM, DARW, and TAHI time series, respectively.

The axial component χ_3 of the AAM computed from the National Centers for Environmental Prediction (NCEP) / National Center for Atmospheric Research (NCAR) reanalysis project available at http://files.aer.com/aerweb/AAM/ with 6-hour sampling interval from January 1948 to March 2019 was used in the analysis (Kalney et al., 1996; Salstein & Rosen, 1997). The axial component in [ms] is computed from

mass + inverted barometer and motion terms by the formula:

$$\chi_3=\chi_{mass+ib}\cdot 0.753/(7.04\cdot 10^{32}\cdot 7.292115\cdot 10^{-5})\cdot 864+\chi_{motion}\cdot 0.998/(7.04\cdot 10^{32}\cdot 7.292115\cdot 10^{-5})\cdot 864$$

3 Wavelet analysis

Wavelet technique is becoming a common tool for analyzing localized variations of power within a time series. By decomposing a time series into the time-frequency domain, one can determine both the dominant modes of variability and how they vary in time (e.g. Daubechies, 1992; Foufoula-Georgiou & Kumar, 1995, 1997; Torrence & Compo, 1998, Grinsted et al., 2004). In this paper, we examine LODR, APM, DARW, THAI and SOI time series by continuous wavelet transform (CWT) and to find a possible connection between atmospheric surface pressure time series and LODR, cross wavelet transform (XWT) was applied (Grinsted et al., 2004).

The LODR, APM, DARW, TAHI, and SOI time series are given in the lower panel of Figs. 1-5, respectively. The CWT power spectra of these time series are shown on the upper panel of Figs. 1-5, respectively. The thick black contour in each CWT power spectrum designates the 5% significance level against red noise and the cone of influence (COI). In the case of LODR, there are obvious annual and semi-annual fluctuations with peaks above the 5% significance level (Fig. 1). The most remarkable oscillation in atmospheric surface pressure variations of APM, DARW, and THAI time series is the annual oscillation exceeding the 5% significance level during the whole time of data (Figs. 2-4). The CWT power spectrum of SOI time series computed from the pressure difference between Darwin and Tahiti stations shows significant ~2 to ~10-year oscillations related to ENSO phenomena and it does not show remarkable annual oscillation which is present in DARW and THAI data.

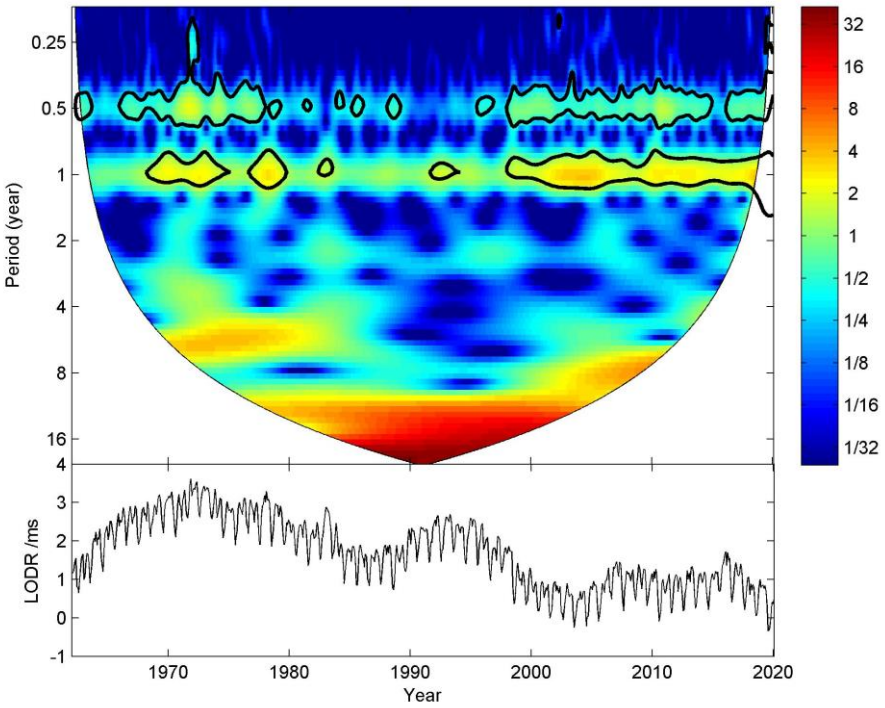

Fig. 1. The LODR time series from January 1962 to January 2020 (lower) and its CWT power spectrum (upper). The thick black contour designates the 5% significance level against red noise and the cone of influence (COI) where edge effects might distort the picture is shown as a white region.

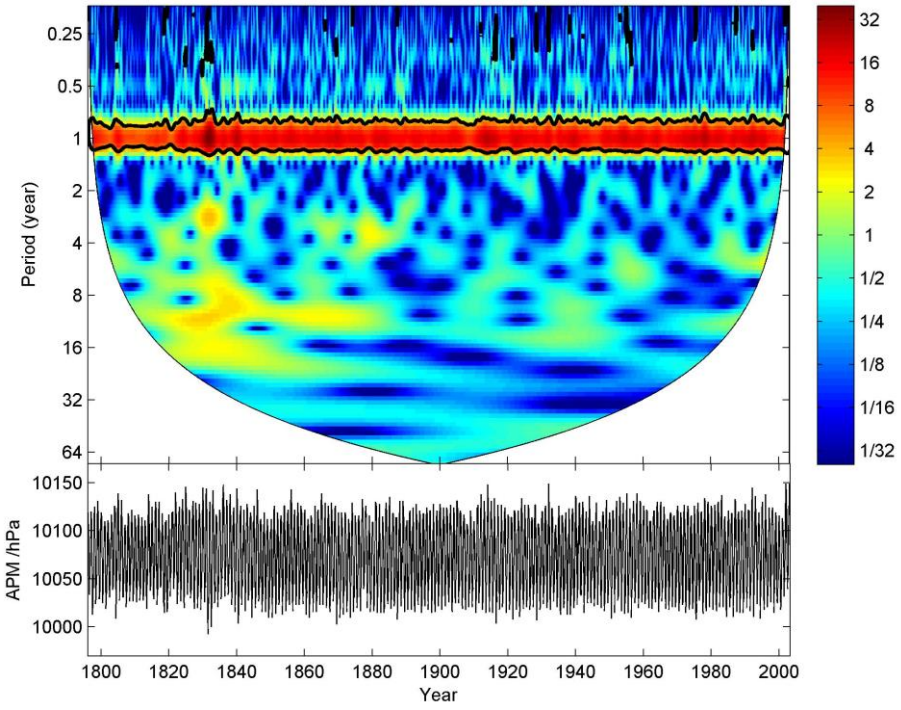

Fig. 2. The APM (lower) time series from January 1796 to March 2003 (lower) and its CWT power spectrum (upper). The explanation of the figure is similar to Fig. 1.

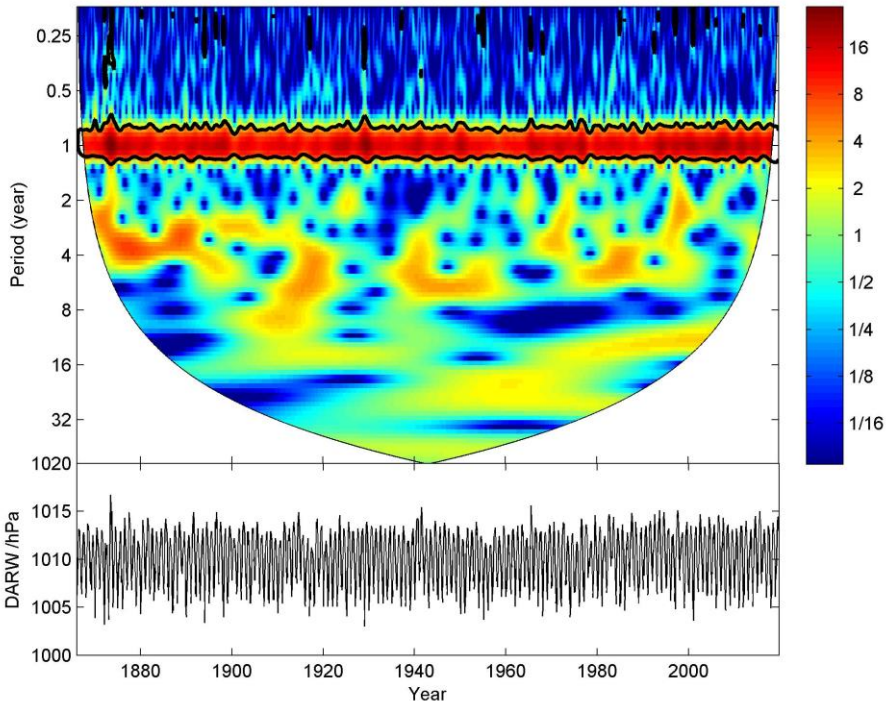

Fig. 3. The DARW (lower) time series from January 1866 to October 2019 and its CWT power spectrum (upper). The explanation of the figure is similar to Fig. 1.

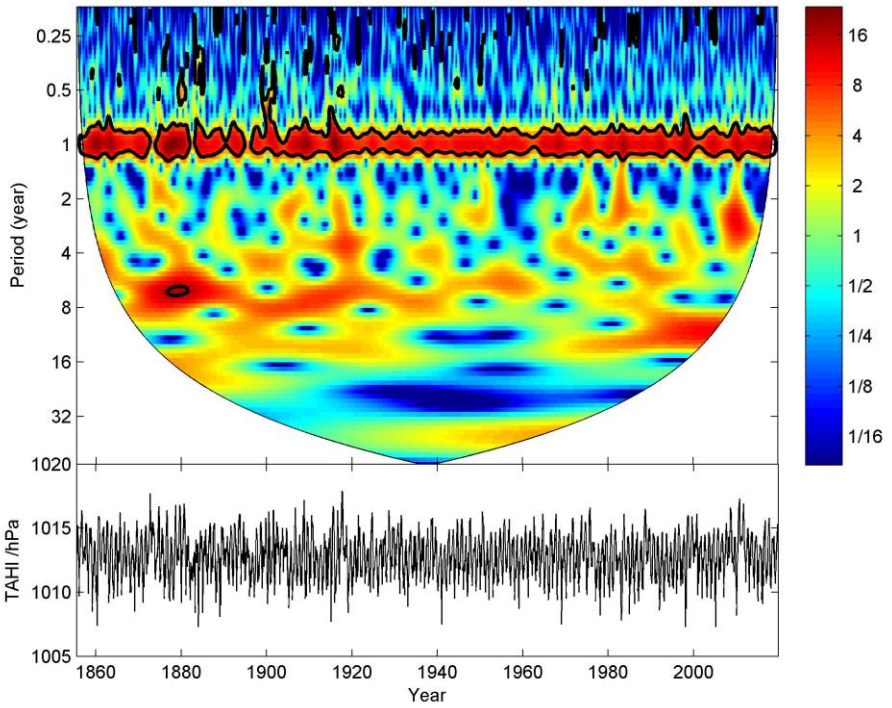

Fig. 4. The TAHI time series from June 1855 to October 2019 (lower) and its CWT power spectrum (upper). The explanation of the figure is similar to Fig. 1.

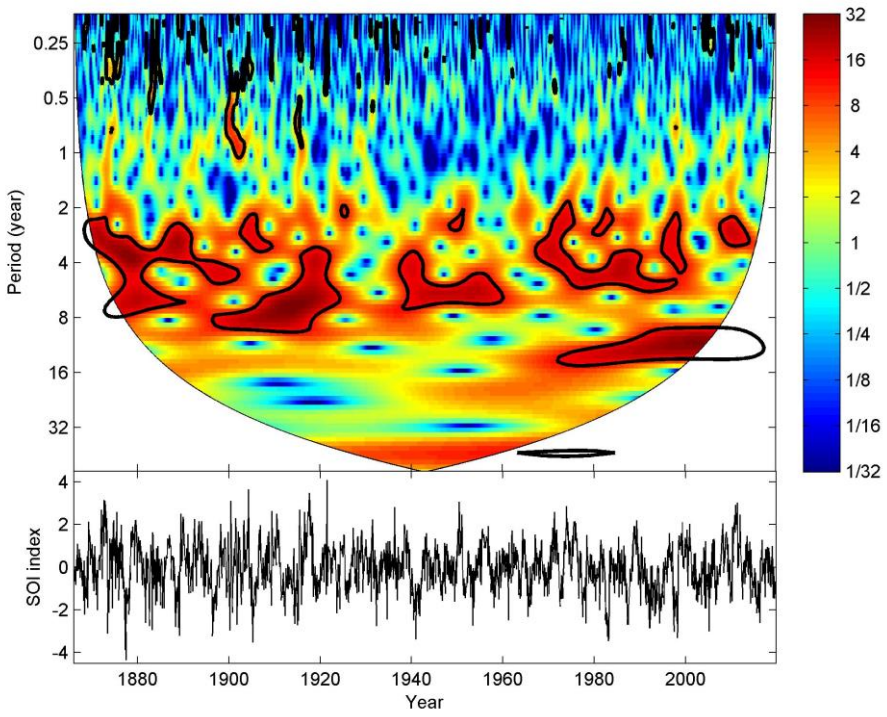

Fig. 5. The SOI time series from January 1866 to October 2019 (lower) and its CWT power spectrum (upper). The explanation of the figure is similar to Fig. 1.

The CWT power spectra do not show a possible connection between the atmospheric surface pressure at chosen meteorological stations near the equator and LODR time series, so the XWT spectra were computed (Figs. 6-8). The remarkable annual signal above the 5% significance level, shown as a thick contour against red noise, can be noticed between atmospheric surface pressure of the APM, DARW, and THAI data and LODR data during the whole time. The phase differences between the frequency components of the considered time series are shown by the directional arrows in the XWT spectrum. The oscillations are in phase when arrows are pointing right, they are 180^{o} out of phase when arrows are pointing left and if the second series leads the first one by 90^{o} the arrows are pointing straight up. It can be noticed that APM is slightly leading LODR during the whole time because the arrows are pointing to the right with a slightly upward direction (Fig. 6). The semi-annual oscillation in the LODR and APM are mostly out of phase because the arrows are generally pointing left (Fig. 6). The annual oscillations in the XWT spectrum of LODR and

DARW (Fig. 7) and the XWT spectrum of LODR and TAHI (Fig. 8) time series are mostly ~180º out of phase. The directions of arrows in the vicinity of the semi-annual oscillation in the XWT spectrum of LODR and DARW are mostly chaotic (Fig. 7) and in the XWT spectrum of LODR and THAI is usually pointing up with a slight left or right direction (Fig. 8). To detect the phase relations between atmospheric surface pressure time series of Darwin and Tahiti with APM data in the whole common data span the XWT spectra between them were computed. The XWT spectra of APM and DARW (Fig. 9) and APM and TAHI (Fig. 10) show that annual oscillations in these pairs are almost ~180º out of phase because the arrows are pointing left with very slight upward direction. It can be also noticed that these XWT spectra show common signals with periods ranging from ~2 to a dozen years associated with ENSO variability (Figs. 9,10).

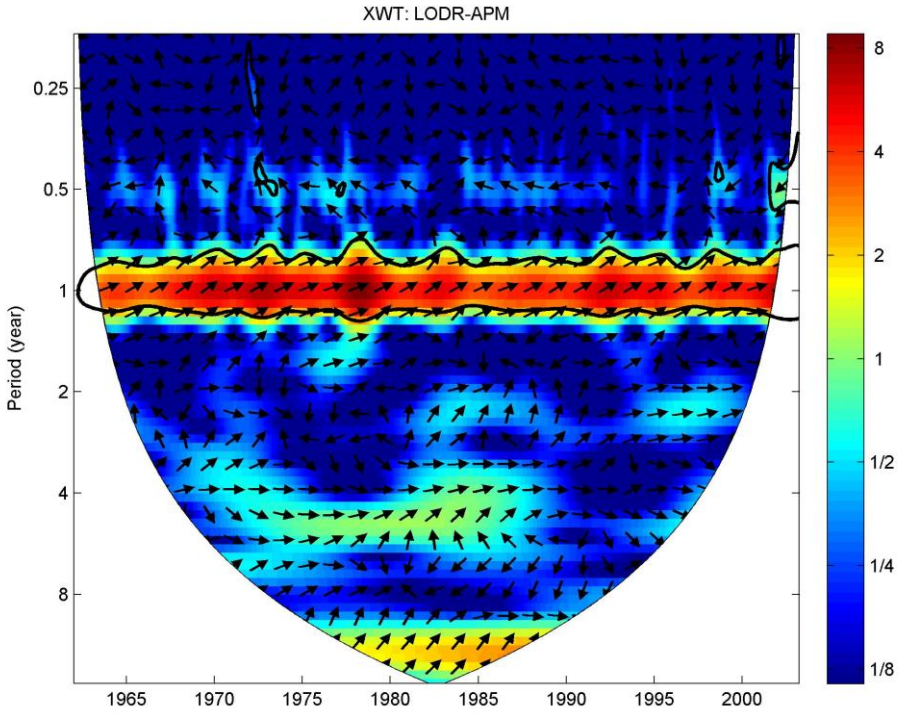

Fig. 6. The XWT spectrum of the LODR and APM time series from January 1962 to March 2003. The 5% significance level against red noise is shown as a thick contour. The relative phase relationship is shown as arrows (with in-phase pointing right, anti-phase pointing left and if APM leads LODR by 90° the arrows are pointing straight up).

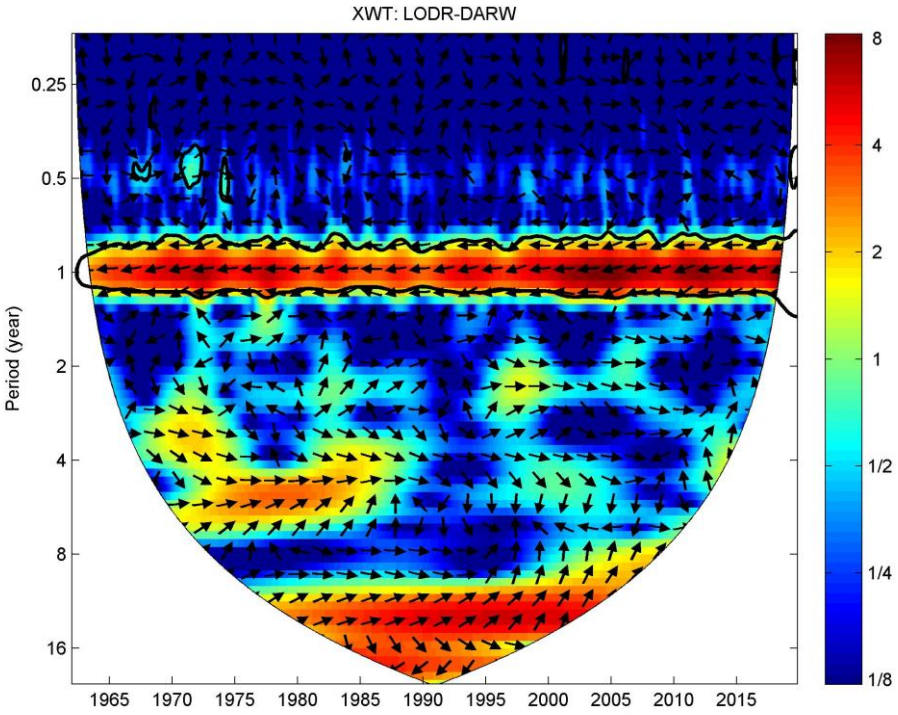

Fig. 7. The XWT spectrum of the LODR and DARW time series from January 1962 to October 2019. The explanation of the figure is similar to Fig. 6.

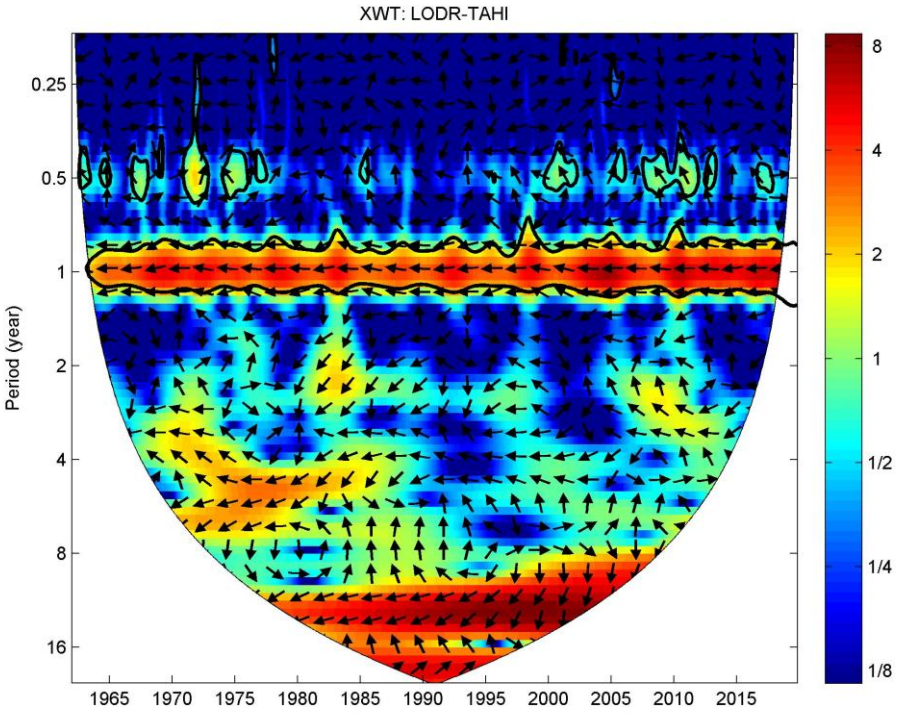

Fig. 8. The XWT spectrum of the LODR and TAHI time series from January 1962 to October 2019. The explanation of the figure is similar to Fig. 6.

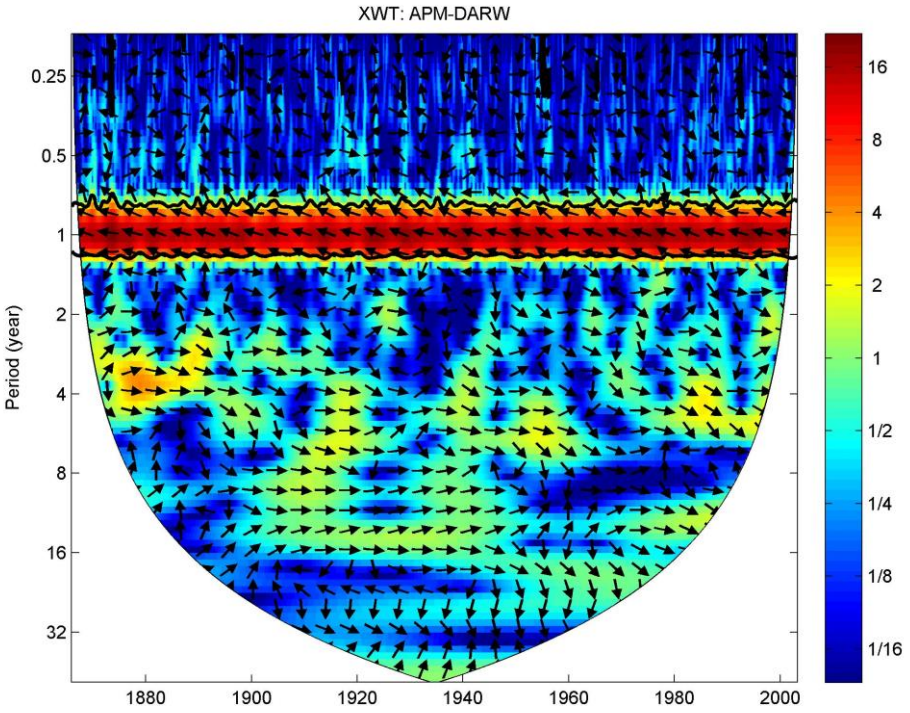

Fig. 9. The XWT spectrum of the APM and DARW time series from January 1866 to March 2003. The explanation of the figure is similar to Fig. 6.

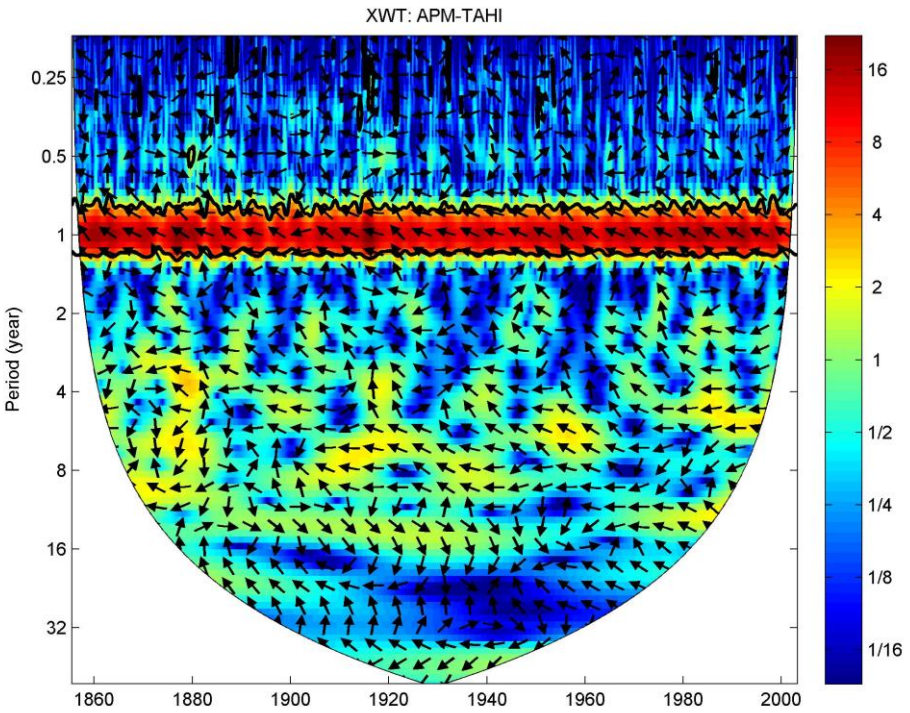

Fig. 10. The XWT spectrum of the APM and TAHI time series from June 1855 to March 2003. The explanation of the figure is similar to Fig. 6.

4 Interannual and intra-seasonal oscillations in LODR, AAM and the atmospheric surface pressure time series

First, all atmospheric surface pressure, LODR, and AAM χ_3 time series were interpolated with the sampling interval of 0.02 years (~1 week) using Lagrange interpolating polynomial of degree 2. Such sampling should not influence the filtration results for oscillations with periods greater than a few weeks. The oscillation with central frequency ω, computed by the FTBPF is given by the following formula:

$$x_t(\omega) = FT^{-1}\left[FT(x(t)) \cdot P(\omega, \mu)\right], \tag{1}$$

where $x(t)$ is a real-valued time series and

$P(\omega,\mu) = \begin{cases} 1-(\omega-\mu)^2/\lambda^2 & if \ \ |\omega-\mu| \le \lambda \\ 0 & otherwise, \end{cases}$ is the parabolic transmittance function in which λ is half of the window bandwidth and μ is the frequency argument. The variable amplitudes and phases of the broadband oscillations can be computed by the FTBPF+HT combination (Kosek et al., 2015, 2020):

$$A_t(\omega) = \sqrt{\Re\left[z_t(\omega)\right]^2 + \Im\left[z_t(\omega)\right]^2}, \tag{2}$$

$$\varphi_t(\omega) = \arctan\left\{\Im\left[z_t(\omega)\right] / \Re\left[z_t(\omega)\right]\right\} - \frac{2\pi t}{T} \tag{3}$$

where

$$z_t(\omega) = FT^{-1}\left[FT(x(t)) \cdot P(\omega, \mu) \cdot (sign(\omega) + 1)\right] \tag{4}$$

is the complex-valued oscillation with the central frequency ω.

To filter the annual oscillations from the atmospheric surface pressure APM, DAWR, and TAHI time series, the FTPBF (Eq. 1) was applied with half of the window bandwidth λ=0.004 (cutoff periods are equal to 0.89 and 1.25 years). The annual oscillations in the DARW and THAI time series are in phase and they are both 180° out of phase with the annual oscillation in the APM time series (Fig. 11) probably due to the opposite direction of Walkers circulation over the Indian and Pacific Oceans.

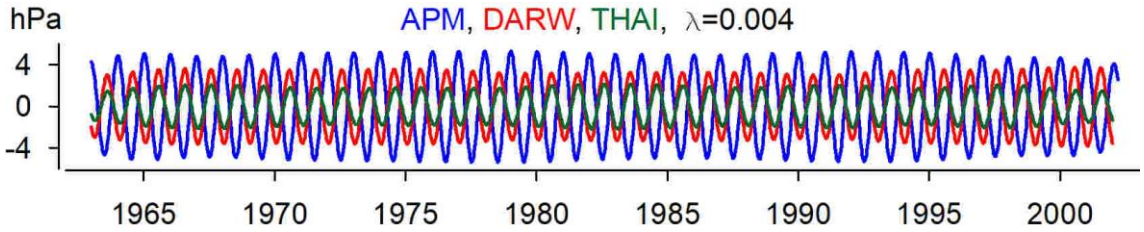

Fig. 11. Annual oscillations in APM (blue), DARW (red), THAI (green), time series computed by the FTBPF with λ=0.004.

The amplitude and phase variations of the annual oscillation computed by the FTBPF+HT (Eqs. 2 and 3) with half of the filter bandwidth λ=0.004 (cutoff periods are equal to 0.89 and 1.25 years) in the LODR and AAM χ_3 time series are very similar (Fig. 12). It should be emphasized that all calculated amplitude and phase variations show errors at the ends of the time series caused by filtration errors of the FTBPF+HT algorithm. To omit these errors caused by filtration, the filtered series were cut off 1 year at the ends. The phase variations of the annual oscillation in the DARW and THAI time series are very close and the phase variations of the annual oscillation in APM time series are slightly greater than the phase variations of these oscillations in LODR and AAM χ_3 time series (Fig. 12). Zero phase crossings for all the considered time series correspond to the same epoch 1957.0. The amplitudes of the annual oscillation in APM, DARW, and THAI time series are variable and are greater for the APM than for the DARW time series which are greater than for THAI time series (Fig. 12). The variable amplitudes of the semi-annual oscillation computed by the FTBPF+HT with half of the filter bandwidth λ=0.004 (cutoff periods are equal to 0.45 to 0.56 years) in APM and DARW time series are of the same order and are about 2 times greater than in the THAI time series (Fig. 13). The variable phases of the semi-annual oscillations in APM and DARW time series are more stable than the phase of the semi-annual oscillation in the THAI time series due to very small amplitude of this oscillation (Fig. 13).

The mean amplitudes and phases of the annual and semi-annual oscillations together with their standard deviations about the mean are shown in Table

1. The mean amplitude of the annual oscillation in the APM time series in 1957.0 - 2002.2 is of the order of 5.1 hPa and the mean amplitudes of the annual oscillation in DARW and THAI time series in 1957.0 - 2018.7 are of the order of 3.4 and 1.8 hPa, respectively.

The amplitude and phase variations of the annual and semi-annual oscillations in LODR and AAM χ_3 time series are very similar (Figs. 12,13), however the mean amplitude of the semi-annual oscillation in AAM χ_3 is about 0.05 ms smaller than in LODR time series (Table 1).

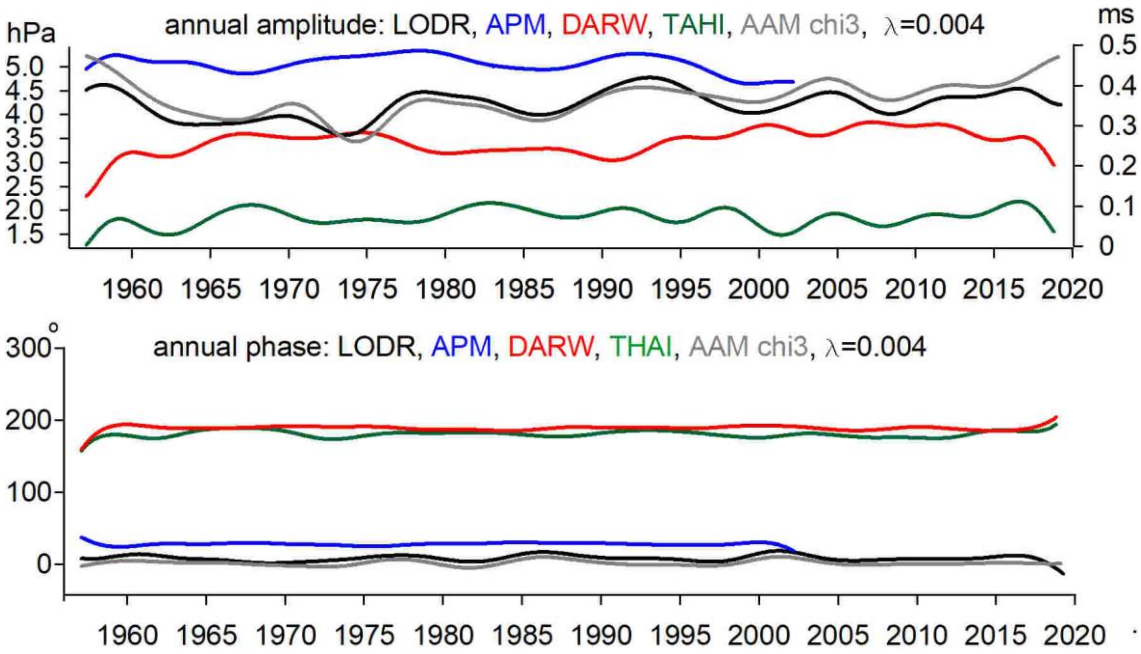

Fig. 12. Variable amplitudes and phases of the annual oscillation computed by the FTBPF+HT with λ=0.004 (cutoff period range: 0.89-1.25 years) in APM (blue), DARW (red), THAI (green) as well as in LODR (black) and AAM χ_3 (grey) time series. The vertical axis for the amplitudes of LODR and AAM χ_3 time series is shown on the right.

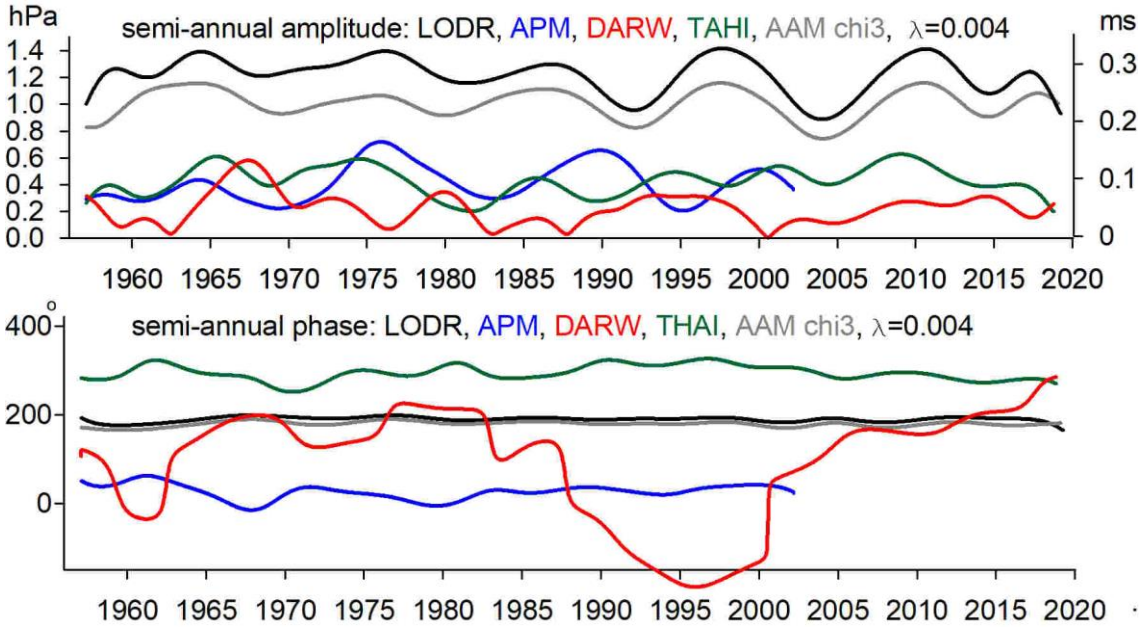

Fig. 13. Variable amplitudes and phases of the semi-annual oscillation computed by the FTBPF+HT with λ=0.004 (cutoff period range: 0.45-0.56 years) in APM (blue), DARW (red), THAI (green), LODR (black), and AAM χ_3 (grey) time series. The vertical axis for the amplitudes of LODR and AAM χ_3 time series is shown on the right.

Table 1. The mean amplitudes and phases of the annual and semi-annual oscillations computed by the FTBPF+HT (λ=0.004) in 1957-2002 in the atmospheric surface pressure time series of Madras, in 1957-2018.7 in the atmospheric surface pressure time series of Darwin and Tahiti as well as in 1957-2019 in LODR, and AAM χ_3 time series together with their standard deviations about the mean.

	Annual		Semi-annual	
	amplitude	phase	amplitude	phase
	[hPa]	[°]	[hPa]	[°]
APM	5.1 ± 0.2	27.6 ± 1.9	0.4 ± 0.1	26.2 ± 16.9
TAHI	1.8 ± 0.2	180.0 ± 4.5	0.4 ± 0.1	294.3 ± 17.0
DARW	3.4 ± 0.2	188.4 ± 3.4	0.2 ± 0.1	93.0 ± 127.0
	[ms]	[°]	[ms]	[°]
LODR	0.35 ± 0.03	8.0 ± 4.3	0.28 ± 0.03	189.5 ± 5.5
AAM χ_3	0.36 ± 0.04	1.4 ± 3.5	0.23 ± 0.02	178.9 ± 5.7

The amplitude variations of oscillations with the central period of 4 years computed by the FTBPF+HT with half of the filter bandwidth λ=0.004 (cutoff periods are equal to 2.2 and 20 years) in the atmospheric surface pressure APM, DAWR and TAHI time series as well as LODR and AAM χ_3 time series are shown in Figure 14. Such filter bandwidth enables filtration of the whole signal in these series related to ENSO variability. It can be

noticed that the amplitude variations of this signal in APM, DARW, and THAI time series are similar. The correlation coefficients between pairs of amplitude variations: APM-DARW and APM-THAI in 1957-2002 are equal to 0.43 and 0.43, respectively and the correlation coefficient between DARW and THAI amplitude variations in 1957-2017.8 is equal to 0.33. The amplitude variations of the 4-year oscillation in atmospheric surface pressure time series are also similar to amplitude variations of such oscillation in LODR and AAM χ_3 time series. The maxima of the amplitude of this wideband oscillation correspond to the biggest El Niño events shown with negative SOI minima in 1982-83, 1997-98, and 2014-15, however other El Niño events in 1972-73 and 2010 could be also noticed (Fig. 14).

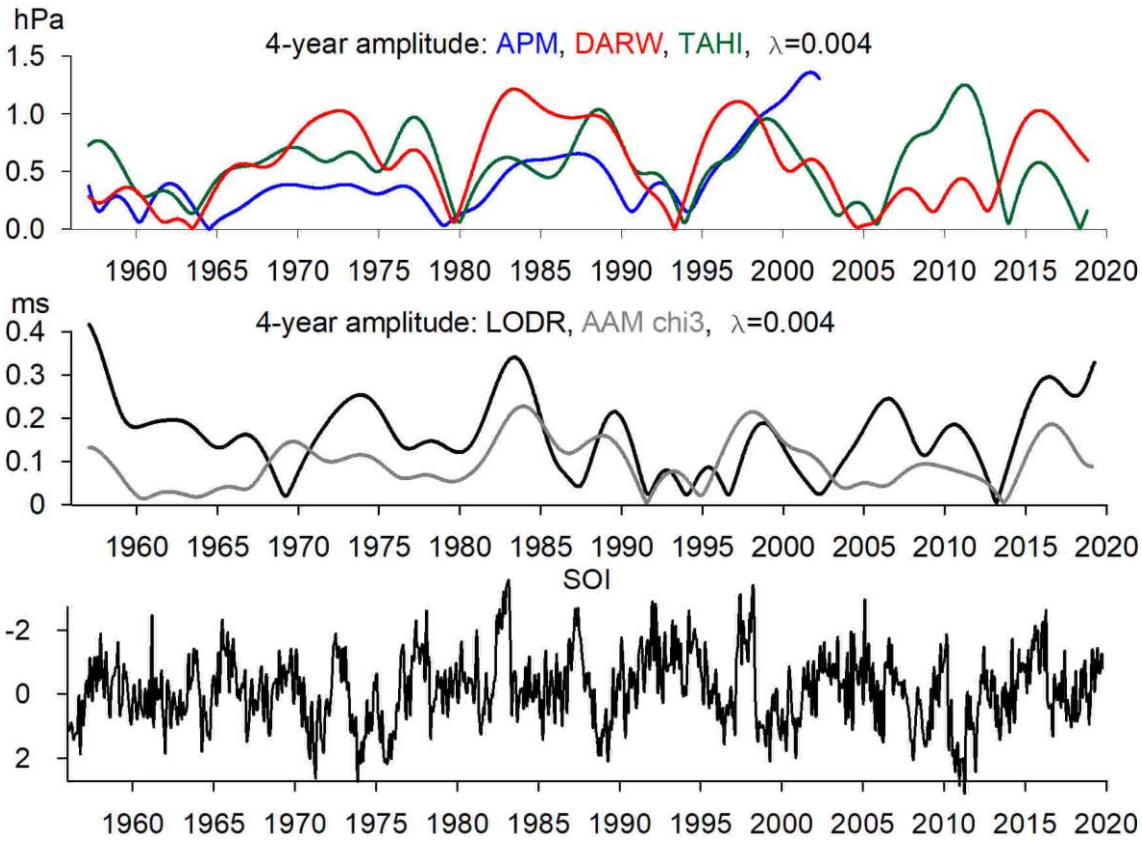

Fig. 14. Variable amplitudes of the 4-year oscillation computed by the FTBPF+HT with λ=0.004 (cutoff period range: 2.2 - 20 years) in APM (blue), DARW (red), THAI (green) as well as in LODR (black) and AAM χ_3 (grey) time series together with the SOI data (black). Note that the scale for SOI is increasing downward.

5 Conclusion and discussion

Annual oscillation is remarkable in atmospheric surface pressure observations of Madras (APM), Darwin (DARW), and Tahiti (TAHI) stations as well as LODR, AAM χ_3 time series. The cross wavelet transform (XWT) spectra revealed, a strong link between LODR and APM, DARW, and TAHI data in the annual frequency band. The XWT spectra and the FTBPF+HT combination revealed that annual oscillations in DARW and THAI time series are in phase from 1957 to 2019 and they are ~180^o out of phase with the annual oscillation in APM time series from 1957 to 2003, probably due to opposite direction of Walker circulation over the Indian and Pacific Oceans. The computed by the FTBPF+HT mean phase of the annual oscillation in APM data is about 20^o greater than in the LODR time series and the mean phases of the annual oscillations in DARW and THAI data is ~180^o out of phase with LODR data. It means that the zonal winds and associated surface pressure changes in Madras have a stimulating effect on the annual oscillations in LODR and AAM χ_3 while the zonal winds and the associated surface pressure changes in Tahiti and Darwin weaken this stimulation. Since the annual oscillation amplitude in atmospheric surface pressure variations of Madras (5.1 hPa) is greater than the amplitudes of the annual oscillations of atmospheric surface pressure changes of Tahiti (1.8 hPa) and Darwin (3.4 hPa) then the phase of annual oscillation in AAM χ_3 and LODR is almost similar to the phase of annual oscillation in surface pressure changes of Madras. Thus, the regions of the Indian Ocean where the Madras station is located may have a greater impact on stimulating the annual oscillation in LODR and AAM than the regions of the Pacific Ocean.

The amplitude and phase variations of the annual and semi-annual oscillation in LODR and AAM χ_3 data computed by the FTBPF+HT combination in 1957-2019 are very similar, however, the mean amplitude of the semi-annual oscillation in AAM χ_3 is about 0.05ms smaller than in LODR data. It suggests that seasonal oscillations in LODR are almost entirely excited by the AAM χ_3 time series. The semi-annual oscillations in

the atmospheric surface pressure of APM and THAI data were detected by the wavelet transform but under the 5% significance level, however, the FTBPF+HT analysis revealed this oscillation with the amplitude of the order of 0.4 hPa and stable phase. The semi-annual oscillation amplitude in the DARW time series is small and negligible because the phase of this oscillation is very unstable.

The amplitude variations of wideband 4-year (from 2.2 to 20 years) signal in APM, DARW and THAI time series related to ENSO phenomena are similar to the amplitude variations of such oscillations in LODR and AAM χ_3 time series. The maxima of the amplitude of this wideband oscillation correspond to the El Niño events in 1972-73, 1982-83, 1997-98, 2010, and 2014-15 years. The detected ~4-year wideband signal in APM data with similar variability as in DARW and THAI data suggests that atmospheric surface pressure variations at Madras station can be an additional indicator of ENSO variability.

Acknowledgments

The authors are grateful to the IERS and Climatic Research Unit (CRU) of the University of East Anglia for providing LODR, APM, DAWR, and TAHI time series, respectively. Wavelet software is provided by C. Torrence and G. Compo and is available at http://paos.colorado.edu/research/wavelets. Software by Grinsted, A., et al., is available at https://github.com/grinsted/wavelet-coherence.

References

Allan, R. J., Reason, C. J. C., Carroll, P. and Jones, P. D.： A reconstruction of Madras (Chennai) mean sea level pressure using instrumental records from the late 18th and early 19th centuries. Int. J. Climatol. 22, 1119-1142 (2002)

Barnes, R. T. H., Hide, R., White, A. A., Wilson, C. A.： Atmospheric angular momentum fluctuations, length of day changes and polar motion, Proc. R. Soc. Lond. A387, 31-74 (1983)

Chao, B. F.: Interannual length-of-day Variation with El Nino/Southern Oscillation/El Nino, Geophys. Res. Lett., 11, 541-544 (1984)

Chao, B. F.: Length-Of-Day Variations Caused by El Niño--Southern Oscillation and Quasi-Biennial Oscillation. Science, 243(4893), 923–925 (1989)

Daubechies, I.: Ten Lectures on Wavelets. SIAM, Philadelphia (1992)

Dickey, J. O., S. L. Marcus, and R. Hide: Global Propagation of Interannual Fluctuations in Atmospheric Angular Momentum, Nature, 357, 484-488 (1992)

Dickey J. O., Marcus S. L., Hide R., Eubanks T. M., Boggs D. H.: Angular momentum exchange among the solid Earth, atmosphere, and oceans: A case study of the 1982-1983 El Niño event. J. Geophys. Res., 99(B12), 23921-23937 (1994)

Foufoula-Georgiou, E., Kumar, P.: Wavelets in Geophysics. Academic Press, San Diego (1994)

Frostman T. O., Martin, D. W., Schwerdtfeger, W.: Annual and semiannual variations in the length of day, related to geophysical effects, Journal of Geophys. Res., 72(20), 5065-5073 (1967)

Gambis, D.: Wavelet Transform Analysis of the Length of the Day and the El Nino/Southern Oscillation Variations at Intraseasonal and Interannual Time Scales, Ann. Geophys, 10, 429-437 (1992)

Gipson J. M. and Ma, C.: Signature of El Niño in length of day as measured by VLBI. IERS Technical Note 26, "The impact of El Nino and other low-frequency Signals on Earth rotation and global Earth system parameters" Salsetein et al. (eds), pp 17-22 (1999)

Grinsted, A., Moore, J. C., Jevrejeva, S.: Application of the cross wavelet transform and wavelet. Nonlinear Process Geophys., 11, 561-566 (2004)

Gross, R. S., Fukumori, I., Menemenlis, D., Gegout, P.: Atmospheric and oceanic excitation of length-of-day variations during 1980–2000, J. Geophys. Res., 109, B01406 (2004)

Höpfner J.: Seasonal variations in length of day and atmospheric angular momentum, Geophysical Journal International, 135(2), 407–437 (1998)

IERS Conventions, Gérard Petit and Brian Luzum (eds.). (IERS Technical Note ; 36) Frankfurt am Main: Verlag des Bundesamts für Kartographie und Geodäsie (2010)

Kalnay, E., et al.: The NCEP/NCAR 40-year reanalysis project. Bull. Amer. Meteor. Soc., 77, 437-471 (1996)

Kosek W., Niedzielski T., Popiński W., Zbylut-Górska M., Wnęk A.: Variable seasonal and subseasonal oscillations in sea level anomaly data and their impact on prediction accuracy, in: International Association of Geodesy Symposia 142, Springer, 2015, pp. 1-6 (2015)

Kosek, W., Popiński, W., Wnęk, A., Sośnica, K., Zbylut-Górska, M.: Analysis of systematic errors in geocenter coordinates determined from GNSS, SLR, DORIS, and GRACE, Pure Appl. Geophys., 177, 867-888 (2020)

Kumar, P., Foufoula-Georgiou, E.: Wavelet analysis for geophysical applications, Rev.

Geophys., 35(4), 385-412 (1997)
Ma, L. H., Han, Y. B.: Atmospheric excitation of time variable length-of-day on seasonal scales. Chin. J. Astron. Astrophys. 6(1), 120-124 (2006a)
Ma, L. H., Liao, D. C., Han, Y. B.: Atmospheric and oceanic excitations to LOD change on quasi-biennial time scales. Chin. J. Astron. Astrophys. 6(6), 759-768 (2006b)
Ropelewski, C. F., Jones, P. D.: An extension of the Tahiti-Darwin Southern Oscillation Index. Monthly Weather Review 115, 2161-2165 (1987)
Rosen, R. D., Salstein, D. A., Eubanks, T. M., Dickey, J. O., Steppe, J. A.: An El Nino signal in atmospheric angular momentum and Earth rotation, Science, 225, 411-414 (1984)
Salstein, D. A., Rosen, R. D.: Earth rotation as a proxy for interannual variability in atmospheric circulation, 1860-present, J. Clim. Appl. Meteorol., 25, 1870-1877 (1986)
Salstein, D. A., Rosen, R. D.: Global momentum and energy signals from reanalysis systems. Preprints, 7th Conf. on Climate Variations, American Meteorological Society, Boston, MA, 344-348 (1997)
Torrence, C., Compo, G. P.: A practical guide to wavelet analysis. Bull. Amer. Meteor. Soc. 79, 61-78 (1998)

Declaration section

Availability of data and materials

All time series used in the analysis are freely available at: the following websites:
SOI and surface pressure of Tahiti and Darwin - https://crudata.uea.ac.uk/cru/data/soi/
Madras MSLP from Rob Allan as in the IJC paper of 2002 - https://crudata.uea.ac.uk/cru/data/madrasmslp/madrasmslp.dat
LODR data - https://hpiers.obspm.fr/iers/series/opa/eopc04R_IAU2000_daily
Wavelet software is available at http://paos.colorado.edu/research/wavelets and at https://github.com/grinsted/wavelet-coherence.
The combination of the Fourier transform band pass filter and the Hilbert transform software was written by Prof. Wieslaw Kosek and Habilitated doctor Waldemar Popinski from Statistics, Poland.

Competing interests

Prof. Lihua Ma is a specialist in Applied Astronomy, Satellite Navigation and Earth Rotation. Prof. Yanben Han was supervisor of PhD thesis of Prof. Lihua Ma. Prof. Wieslaw Kosek is a specialist in application of time series analysis methods to analysis of Earth Orientation Parameters and their geophysical excitation functions, altimetric sea level variations and geocenter coordinates. The manuscript was written through contributions of all authors. All authors have given approval to the final version of the manuscript. All authors do not have any possible conflicts of interest.

Funding

Statutory funds of Faculty of Civil Engineering and Geodesy, Military University of Technology, Warsaw, Poland.

Authors' contributions

Lihua Ma gave wavelet analysis and corresponding results shown in Figures 1-10 of all data series. His contributions mainly are located in Section 1: Introduction and Section 3: Wavelet analysis.

Wieslaw Kosek provided analysis by combination of the Fourier Transform band pass filter and the Hilbert transform shown in Figures 11-14 and in Table 1. His contributions mainly are located in Section 1: Introduction and Section 4: Interannual and intra-seasonal oscillations in LODR, AAM and the atmospheric surface pressure time series.

Yanben Han gave preliminary paper ideas and made some discussion about results. His contributions mainly are located in Section 1: Introduction and Section 5: Conclusion and discussion.

Acknowledgements

The authors are grateful to the IERS and Climatic Research Unit (CRU) of the University of East Anglia for providing LODR, APM, DAWR, and TAHI time series, respectively. Wavelet software is provided by C. Torrence and G. Compo and is available at http://paos.colorado.edu/research/wavelets. Software by Grinsted, A., et al., is available at https://github.com/grinsted/wavelet-coherence.

Figures

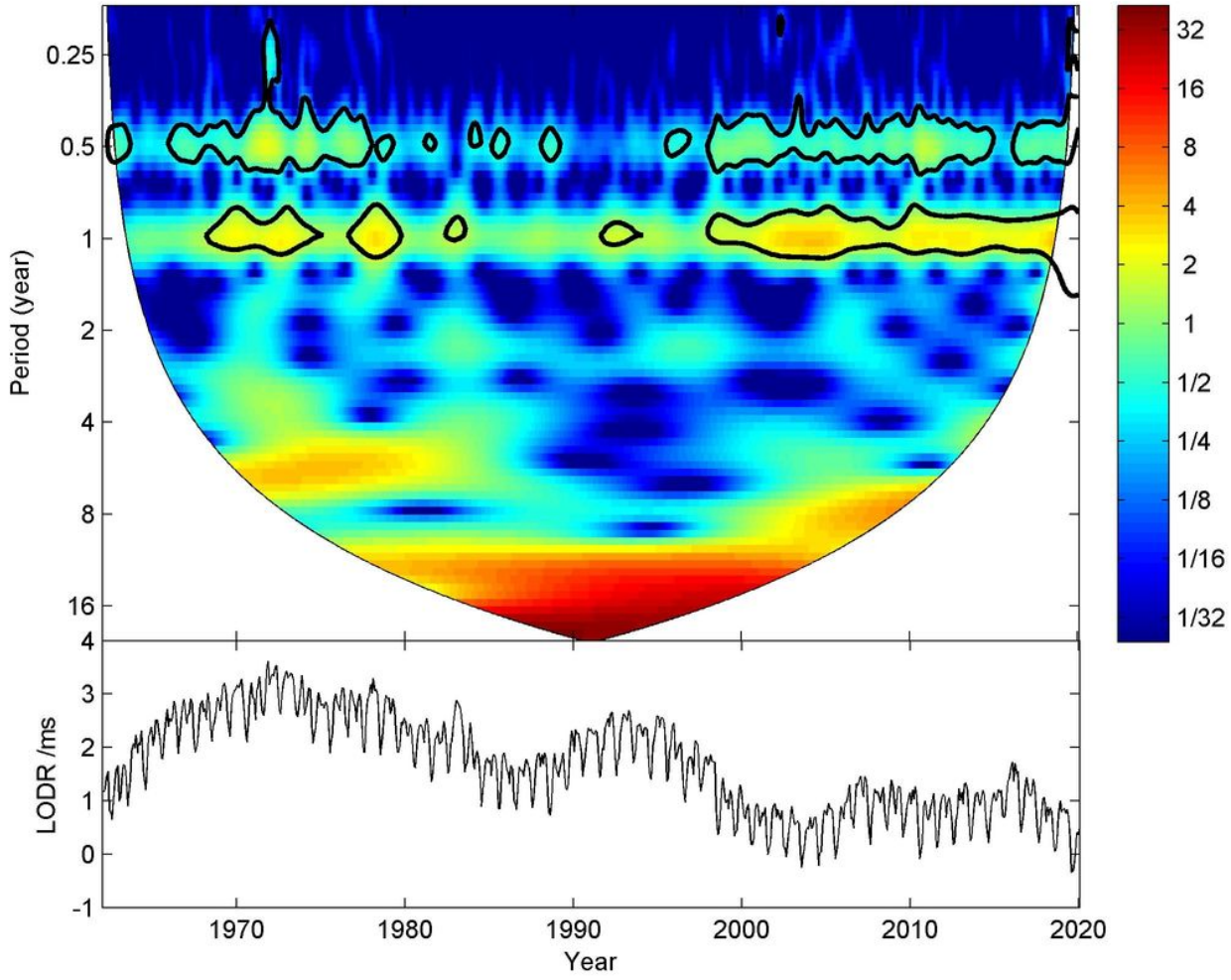

Figure 1

The LODR time series from January 1962 to January 2020 (lower) and its CWT power spectrum (upper). The thick black contour designates the 5% significance level against red noise and the cone of influence (COI) where edge effects might distort the picture is shown as a white region.

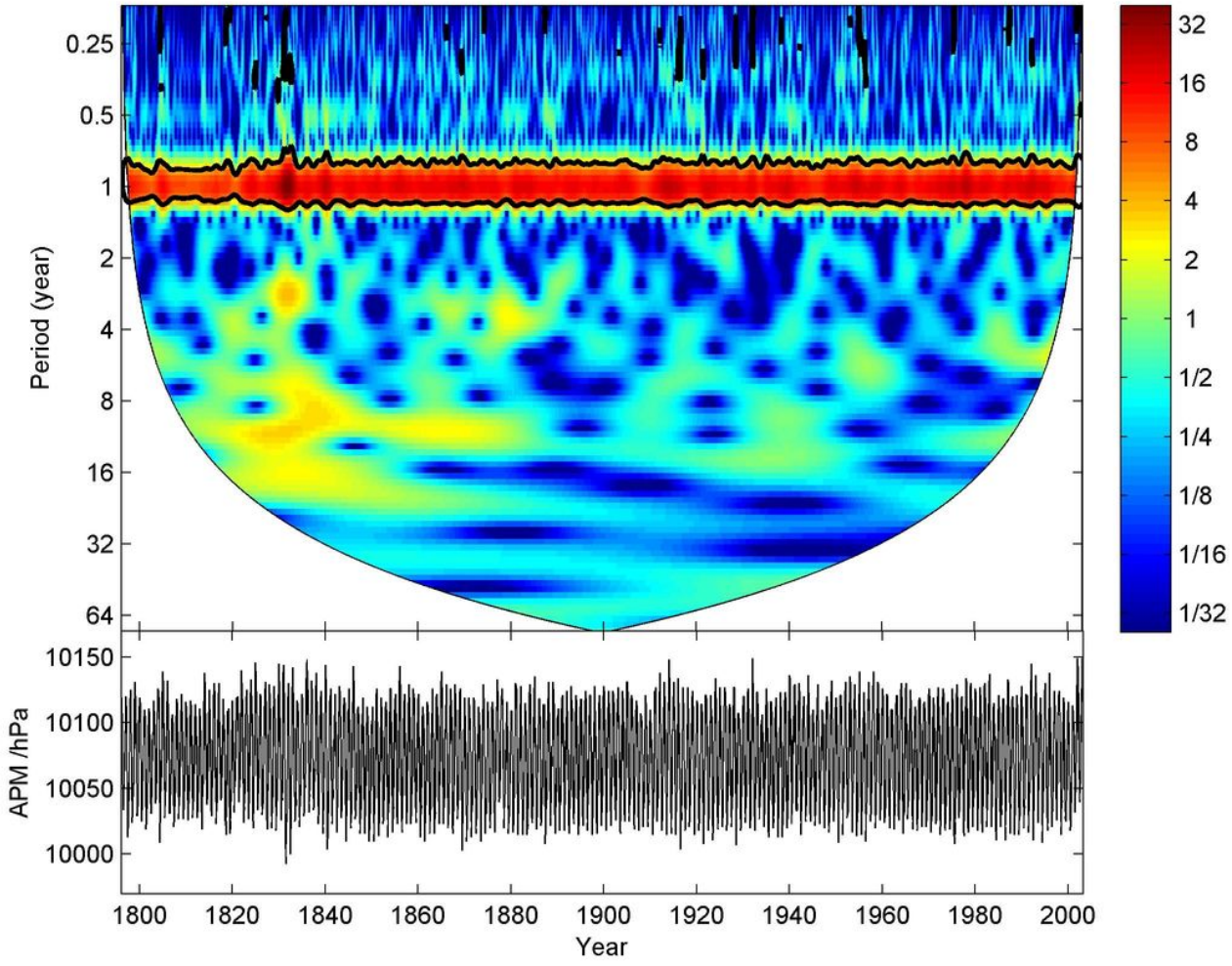

Figure 2

The APM (lower) time series from January 1796 to March 2003 (lower) and its CWT power spectrum (upper). The explanation of the figure is similar to Fig. 1.

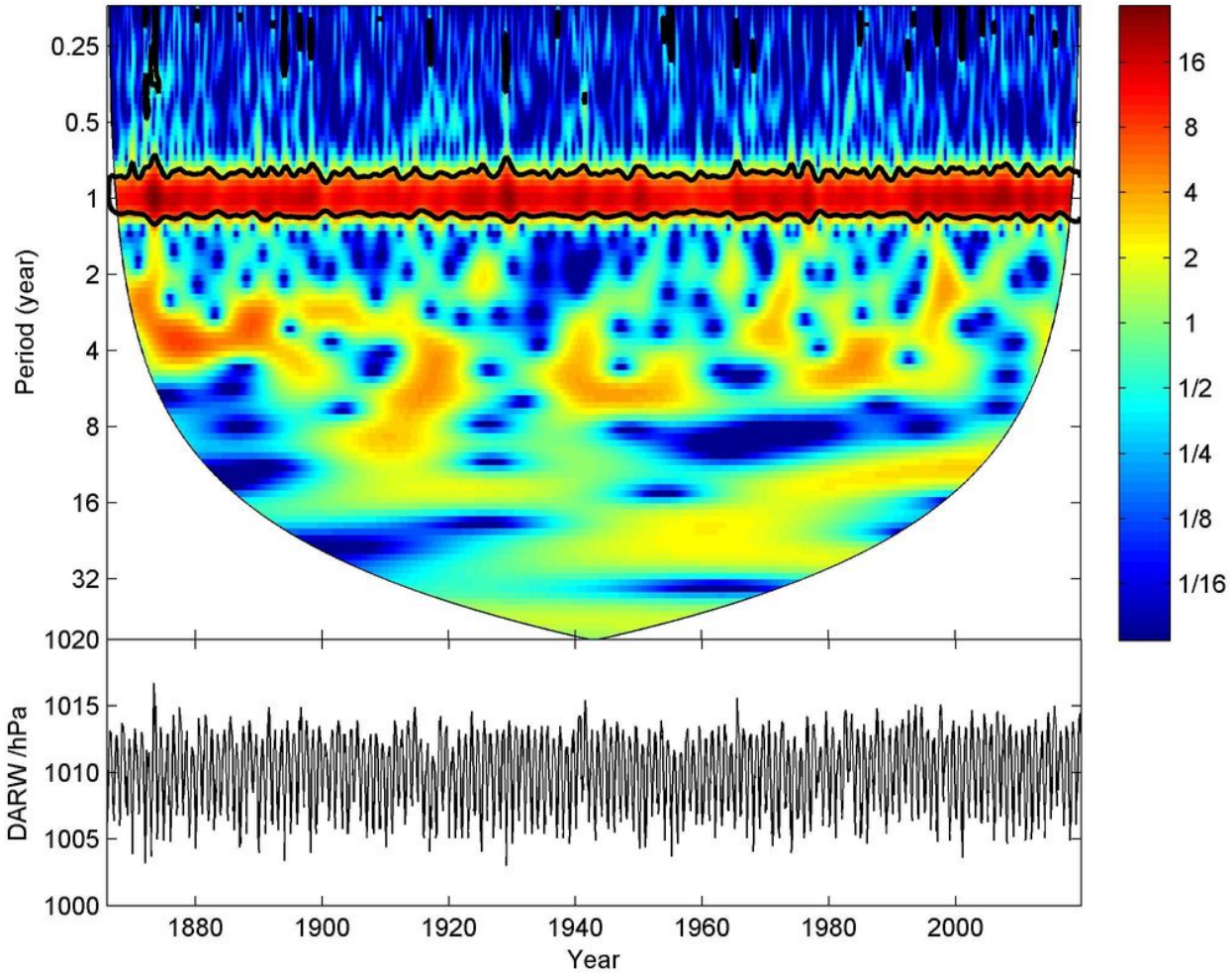

Figure 3

The DARW (lower) time series from January 1866 to October 2019 and its CWT power spectrum (upper). The explanation of the figure is similar to Fig. 1.

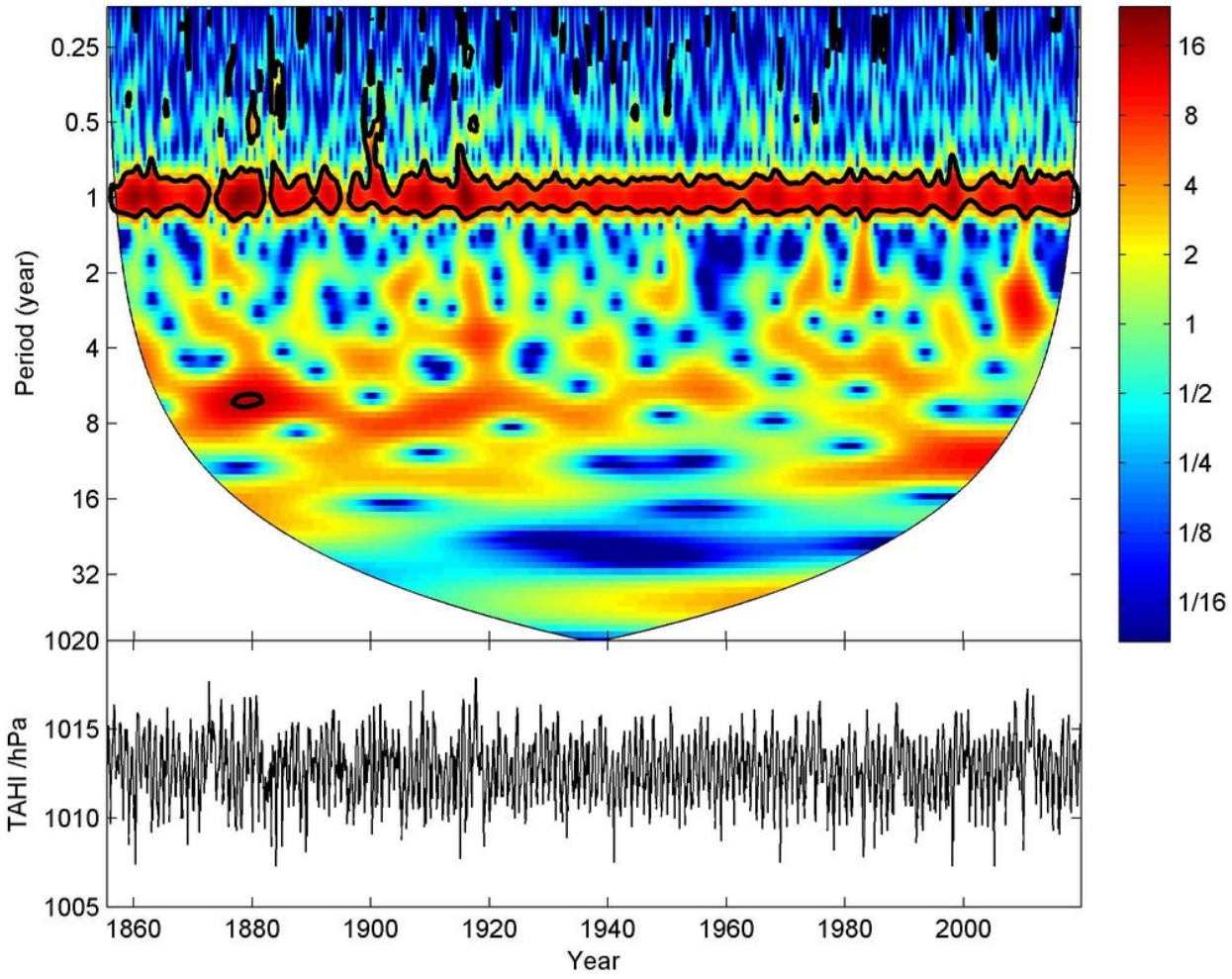

Figure 4

The TAHI time series from June 1855 to October 2019 (lower) and its CWT power spectrum (upper). The explanation of the figure is similar to Fig. 1.

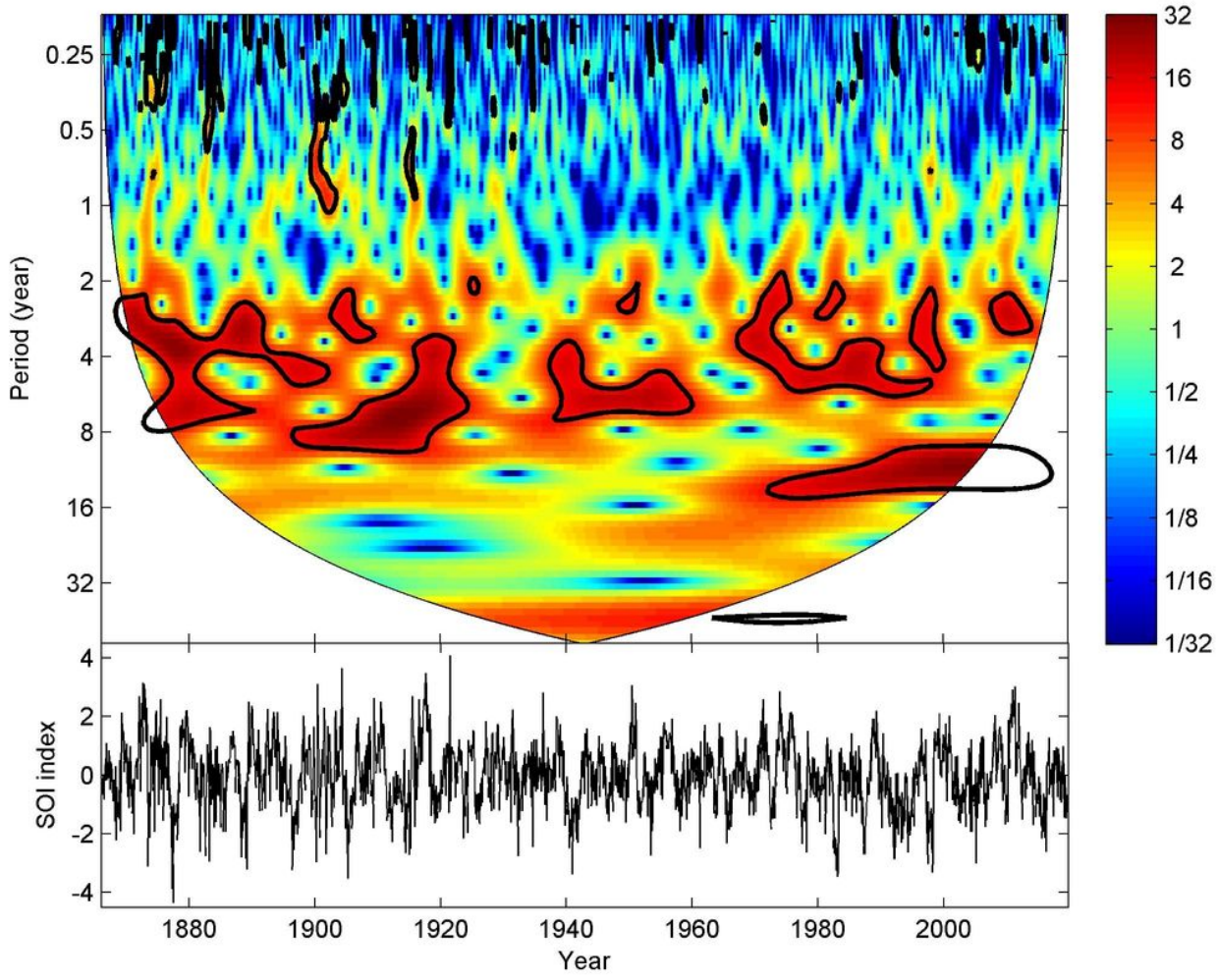

Figure 5

The SOI time series from January 1866 to October 2019 (lower) and its CWT power spectrum (upper). The explanation of the figure is similar to Fig. 1.

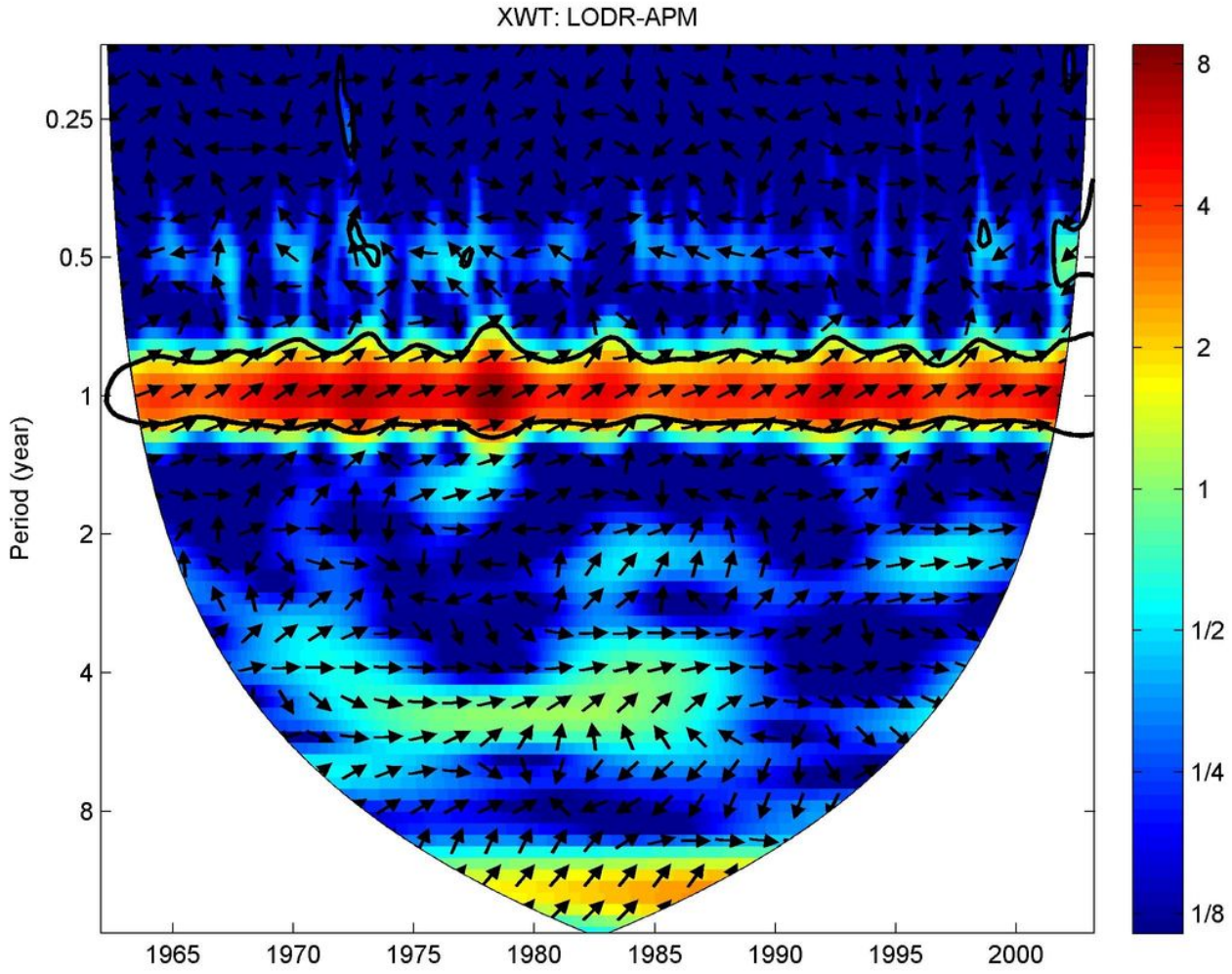

Figure 6

The XWT spectrum of the LODR and APM time series from January 1962 to March 2003. The 5% significance level against red noise is shown as a thick contour. The relative phase relationship is shown as arrows (with in-phase pointing right, anti-phase pointing left and if APM leads LODR by 90° the arrows are pointing straight up).

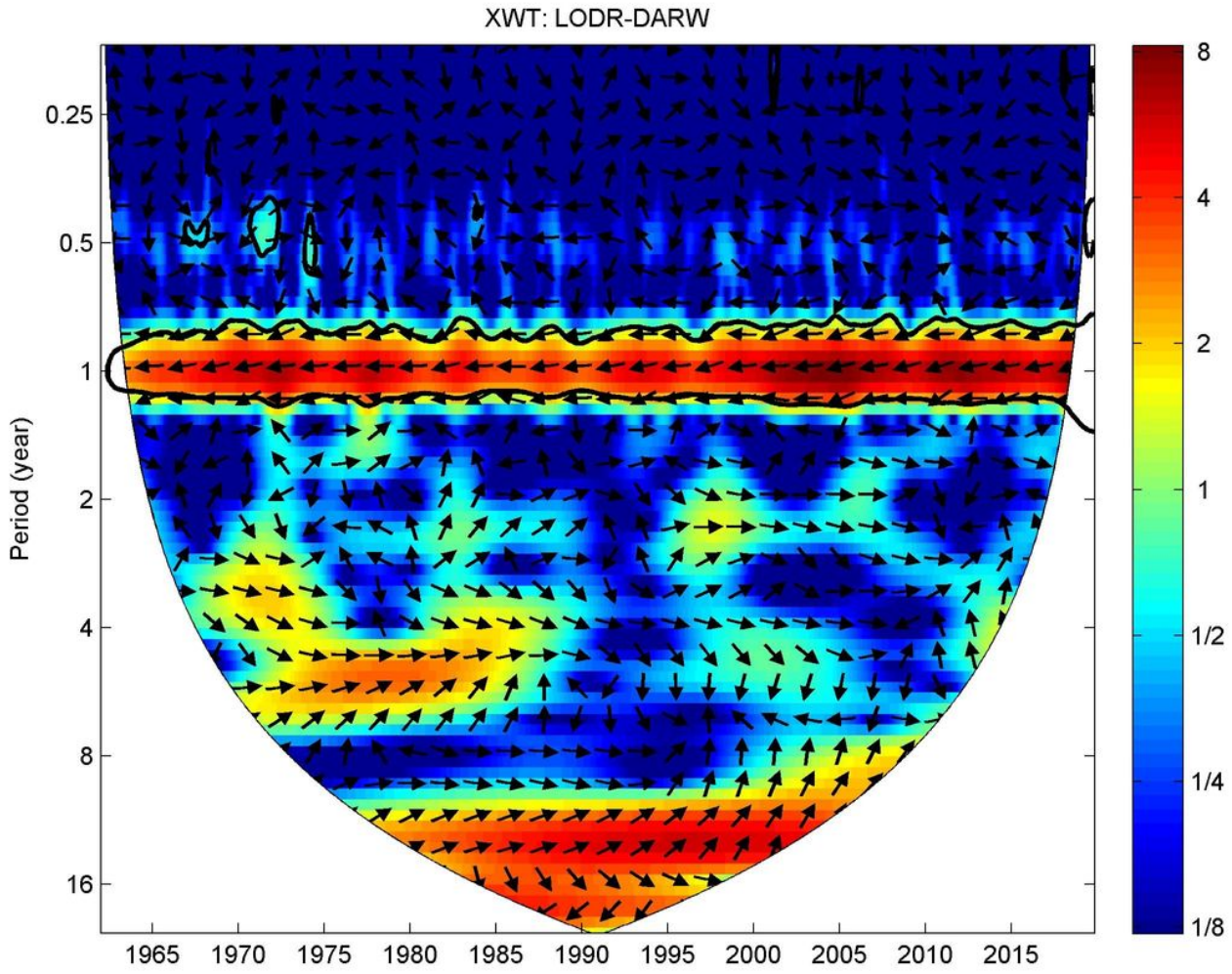

Figure 7

The XWT spectrum of the LODR and DARW time series from January 1962 to October 2019. The explanation of the figure is similar to Fig. 6.

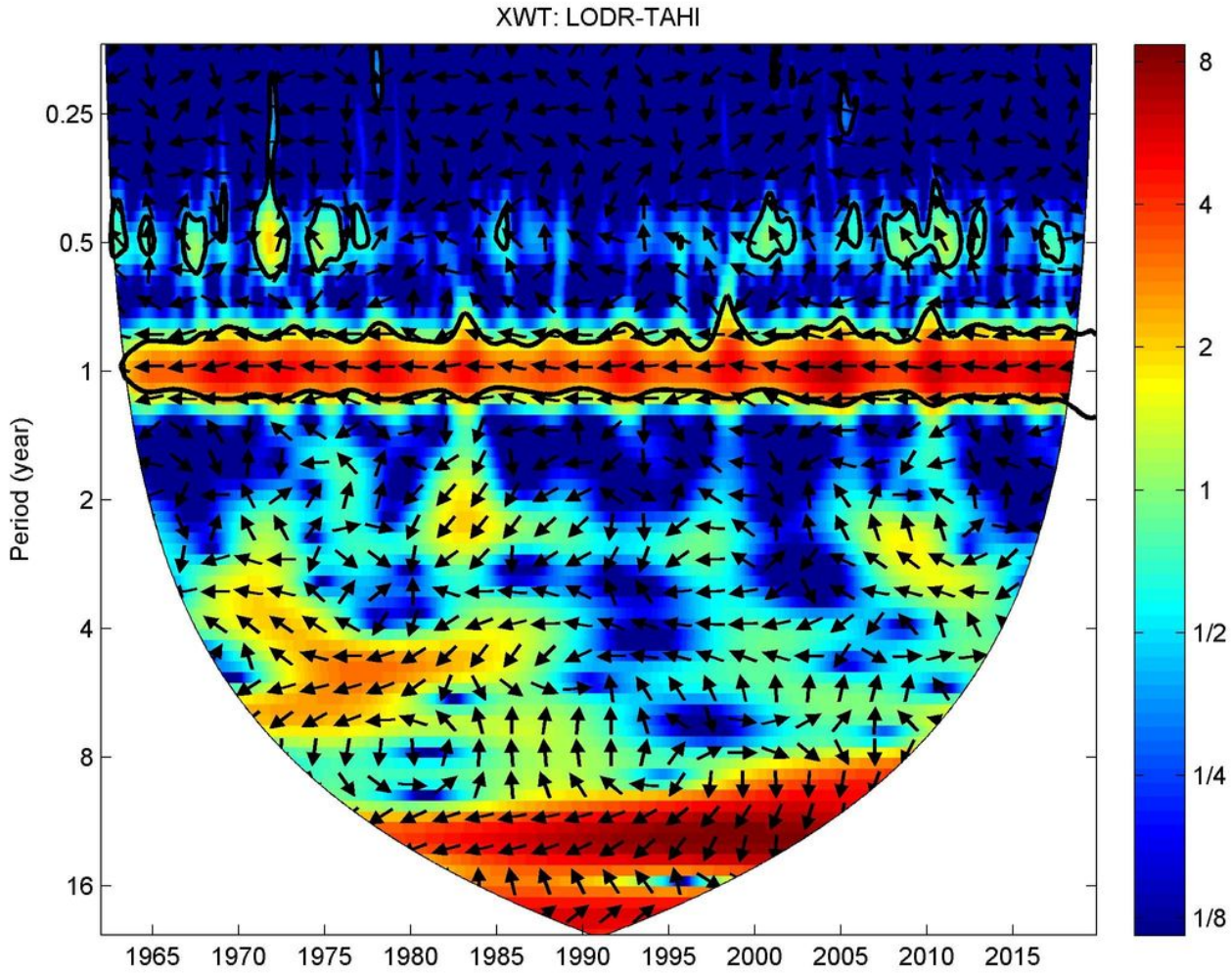

Figure 8

The XWT spectrum of the LODR and TAHI time series from January 1962 to October 2019. The explanation of the figure is similar to Fig. 6.

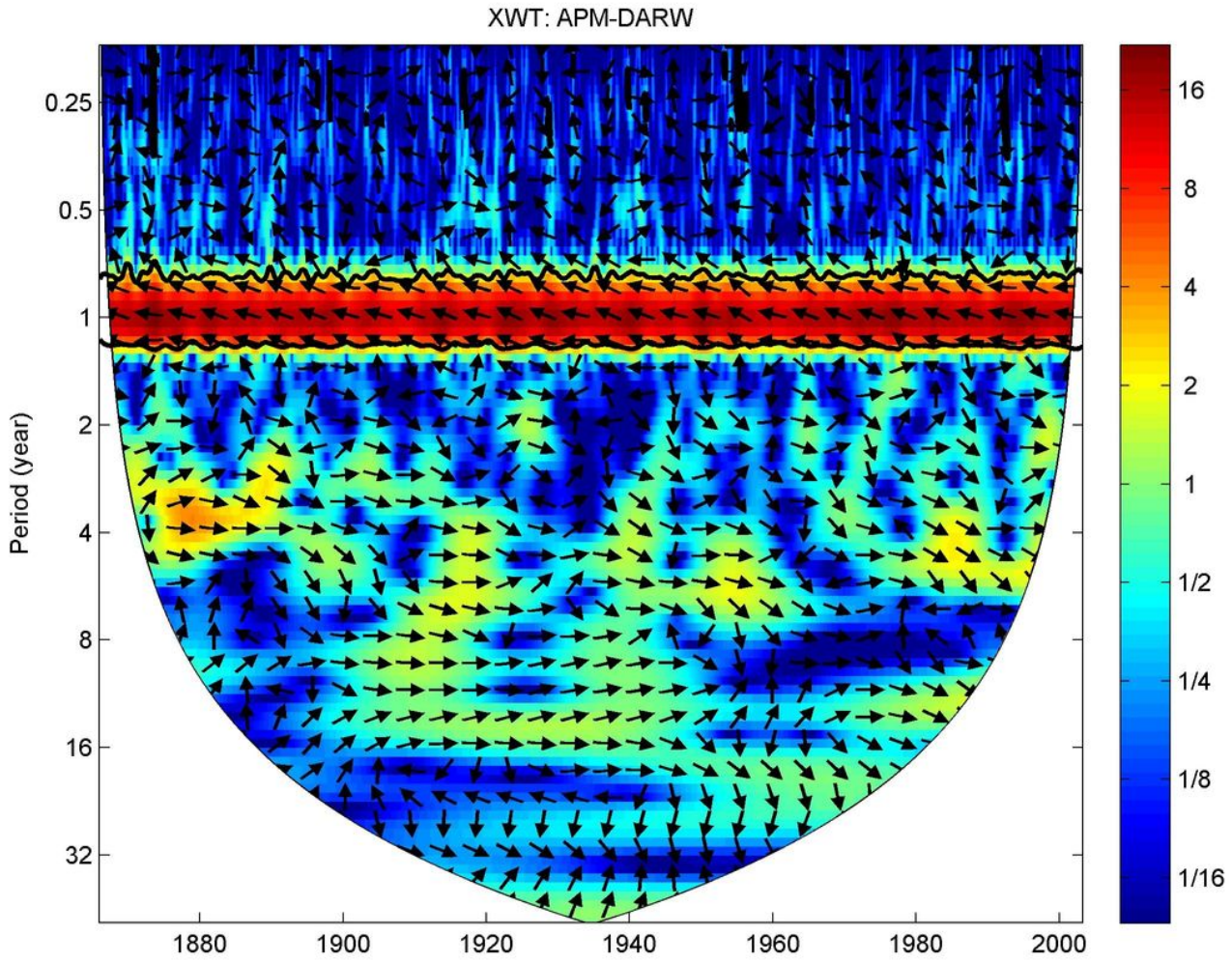

Figure 9

The XWT spectrum of the APM and DARW time series from January 1866 to March 2003. The explanation of the figure is similar to Fig. 6.

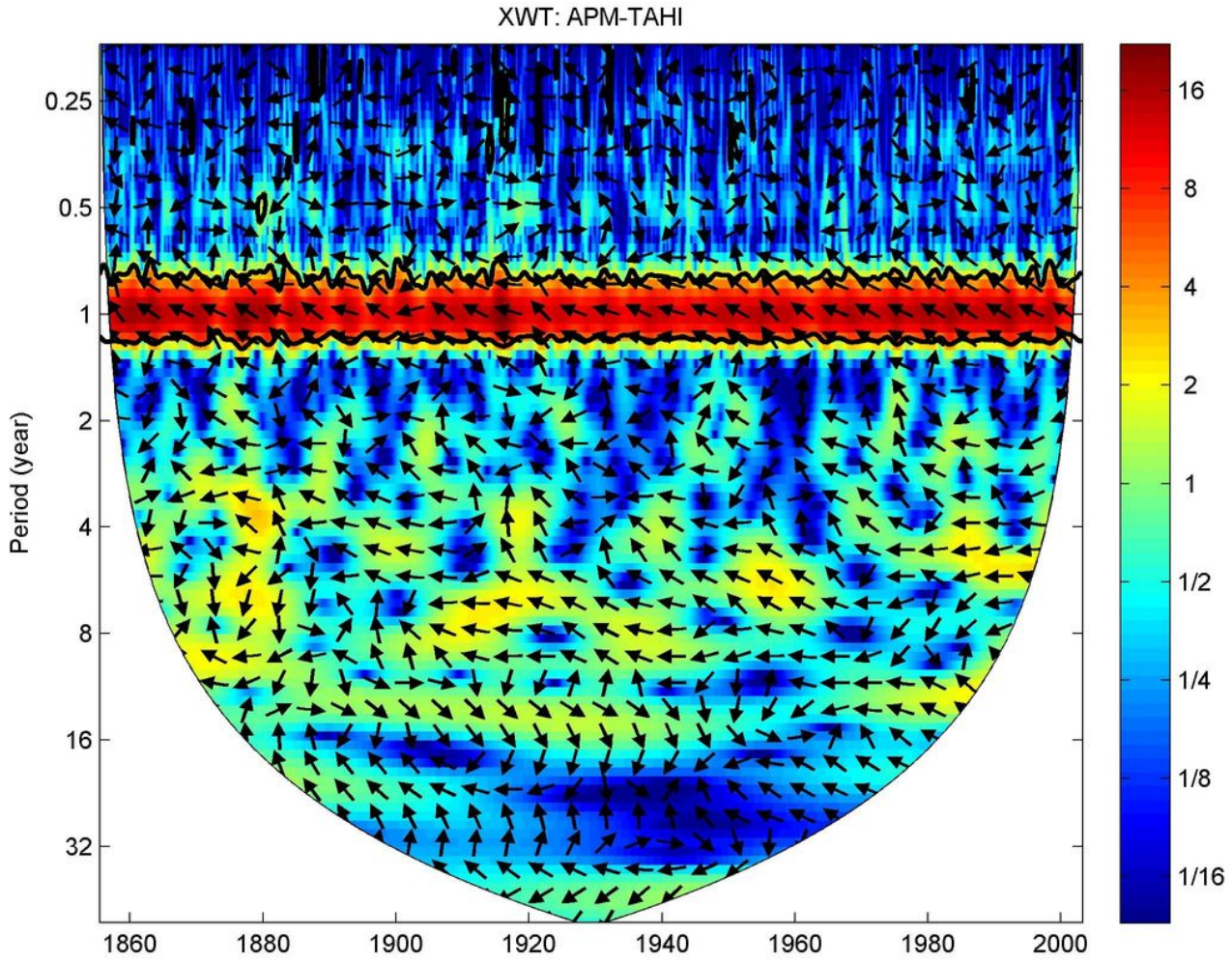

Figure 10

The XWT spectrum of the APM and TAHI time series from June 1855 to March 2003. The explanation of the figure is similar to Fig. 6.

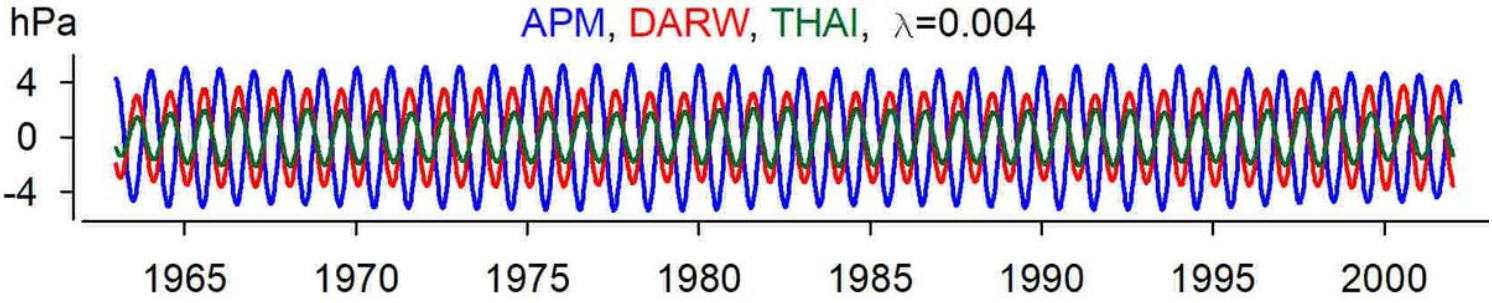

Figure 11

Annual oscillations in APM (blue), DARW (red), THAI (green), time series computed by the FTBPF with λ=0.004.

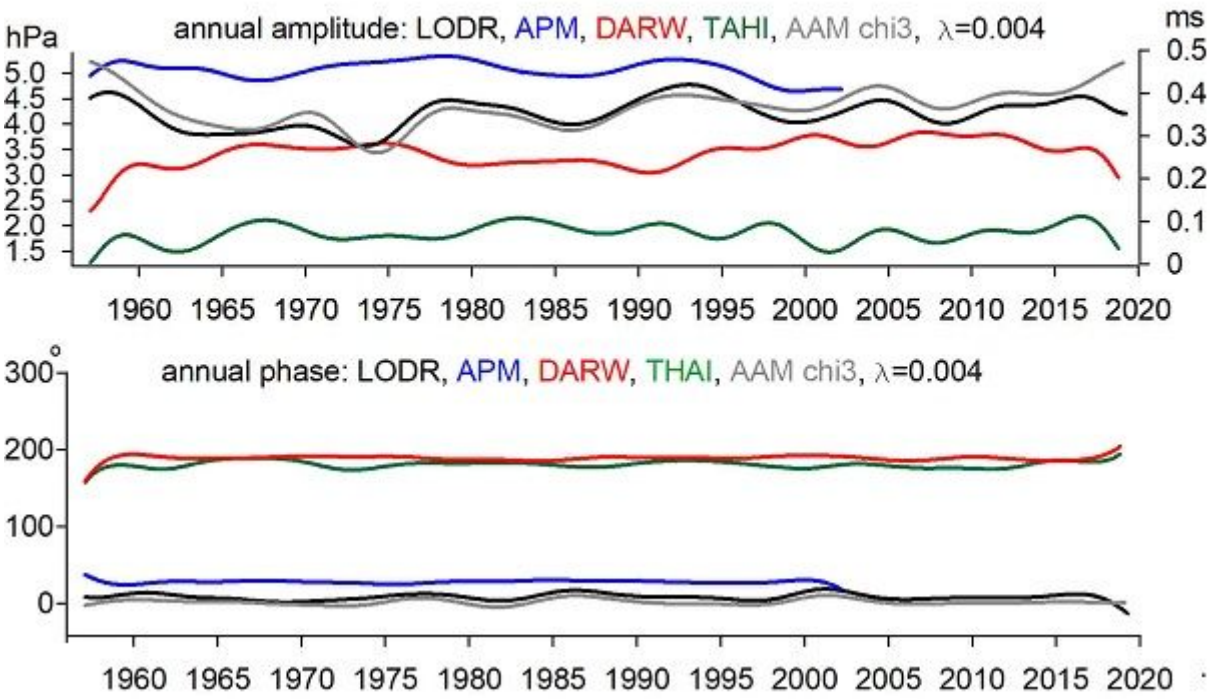

Figure 12

Variable amplitudes and phases of the annual oscillation computed by the FTBPF+HT with λ=0.004 (cutoff period range: 0.89-1.25 years) in APM (blue), DARW (red), THAI (green) as well as in LODR (black) and AAM χ3 (grey) time series. The vertical axis for the amplitudes of LODR and AAM χ3 time series is shown on the right.

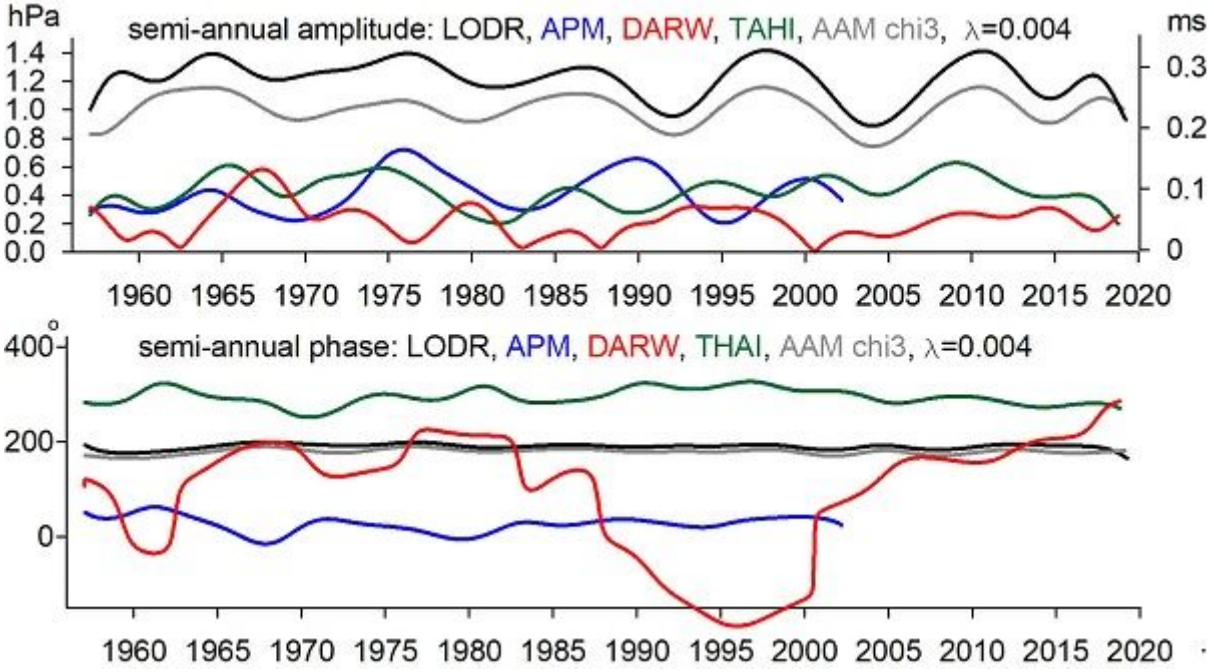

Figure 13

Variable amplitudes and phases of the semi-annual oscillation computed by the FTBPF+HT with λ=0.004 (cutoff period range: 0.45-0.56 years) in APM (blue), DARW (red), THAI (green), LODR (black), and AAM χ3 (grey) time series. The vertical axis for the amplitudes of LODR and AAM χ3 time series is shown on the right.

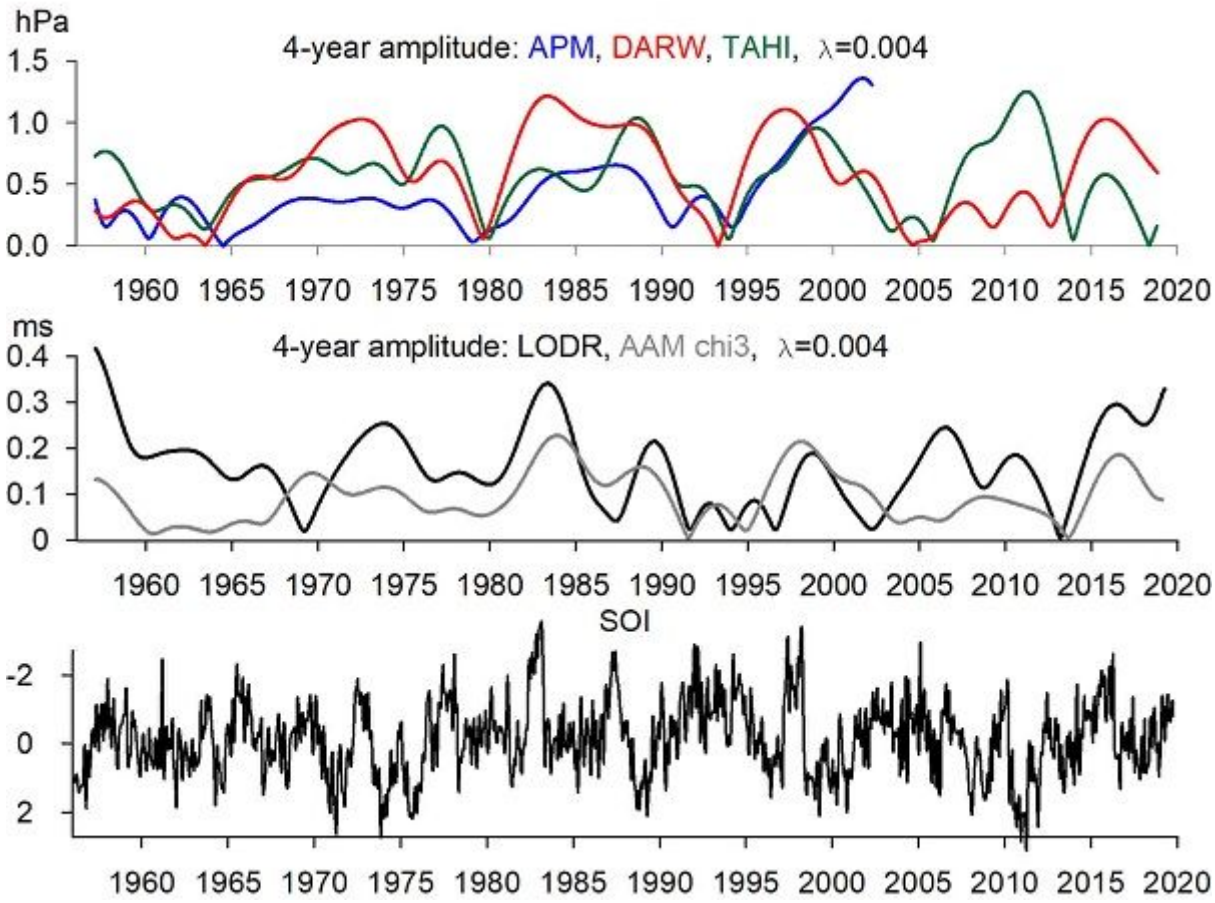

Figure 14

Variable amplitudes of the 4-year oscillation computed by the FTBPF+HT with λ=0.004 (cutoff period range: 2.2 - 20 years) in APM (blue), DARW (red), THAI (green) as well as in LODR (black) and AAM χ3 (grey) time series together with the SOI data (black). Note that the scale for SOI is increasing downward.

Supplementary Files

This is a list of supplementary files associated with this preprint. Click to download.

- ABS1m.jpg